

QUASI-PERIODIC TRAVELING GRAVITY-CAPILLARY WAVES

JON WILKENING AND XINYU ZHAO

ABSTRACT. We present a numerical study of spatially quasi-periodic traveling waves on the surface of an ideal fluid of infinite depth. This is a generalization of the classic Wilton ripple problem to the case when the ratio of wave numbers satisfying the dispersion relation is irrational. We develop a conformal mapping formulation of the water wave equations that employs a quasi-periodic variant of the Hilbert transform to compute the normal velocity of the fluid from its velocity potential on the free surface. We develop a Fourier pseudo-spectral discretization of the traveling water wave equations in which one-dimensional quasi-periodic functions are represented by two-dimensional periodic functions on the torus. This leads to an overdetermined nonlinear least squares problem that we solve using a variant of the Levenberg-Marquardt method. We investigate various properties of quasi-periodic traveling waves, including Fourier resonances and the dependence of wave speed and surface tension on the amplitude parameters that describe a two-parameter family of waves.

1. INTRODUCTION

Traveling water waves have long played a central role in the field of fluid mechanics. Spatially periodic traveling waves, dating back to Stokes [11, 33], have been studied extensively [6, 21–24, 29, 30, 34]. However, little research has been done on spatially quasi-periodic water waves in spite of their abundance in integrable model water wave equations such as the Korteweg-de Vries equation and the nonlinear Schrödinger equation. On the theoretical side, Bridges and Dias [8] used a spatial Hamiltonian structure to construct weakly nonlinear approximations of spatially quasi-periodic traveling gravity-capillary waves for two special cases: deep water and shallow water. The existence of such waves in the fully nonlinear setting is still an open problem. In this paper, we formulate the quasi-periodic traveling wave problem in a conformal mapping framework, demonstrate their existence numerically, and explore their properties.

To motivate our work, recall the dispersion relation for linearized traveling gravity-capillary waves in deep water:

$$(1.1) \quad c^2 = gk^{-1} + \tau k.$$

Here c is the phase speed, k is the wave number, g is the acceleration due to gravity and τ is the coefficient of surface tension. Notice that $c = \sqrt{(g/k) + \tau k}$ has a positive minimum, denoted by c_{crit} . For any fixed phase speed $c > c_{\text{crit}}$, there are two distinct positive wave numbers satisfying the dispersion relation (1.1), denoted k_1 and k_2 . Any traveling solution of the linearized problem with this speed can be expressed as a superposition of waves with these wave numbers. If k_1 and k_2 are rationally related, the motion is spatially periodic

This work was supported in part by the National Science Foundation under award number DMS-1716560 and by the Department of Energy, Office of Science, Applied Scientific Computing Research, under award number DE-AC02-05CH11231.

and corresponds to the well-known Wilton ripples [1, 35, 39]. However, if k_1 and k_2 are irrationally related, the motion will be spatially quasi-periodic.

Recently, Berti *et al* [5, 7] have proved the existence of small-amplitude temporally quasi-periodic gravity-capillary waves using Nash-Moser theory. They show that solutions of the linearized standing water wave problem can be combined and perturbed to obtain temporally quasi-periodic solutions of the nonlinear problem. Following the same philosophy, we look for spatially quasi-periodic solutions of the traveling water wave equations that are perturbations of solutions of the linearized problem. The velocity potential can be eliminated from the Euler equations when looking for traveling solutions, so our goal is to study traveling waves with height functions of the form

$$(1.2) \quad \eta(\alpha) = \tilde{\eta}(k_1\alpha, k_2\alpha), \quad \tilde{\eta}(\alpha_1, \alpha_2) = \sum_{(j_1, j_2) \in \mathbb{Z}^2} \hat{\eta}_{j_1, j_2} e^{i(j_1\alpha_1 + j_2\alpha_2)}.$$

Here $\tilde{\eta}$ is real-valued and defined on the torus $\mathbb{T}^2 = \mathbb{R}^2/2\pi\mathbb{Z}^2$, and α parametrizes the free surface in such a way that the fluid domain is the image of the lower half-plane $\{w = \alpha + i\beta : \beta < 0\}$ under a conformal map $z(w)$ whose imaginary part on the upper boundary is $\text{Im}\{z|_{\beta=0}\} = \eta$. The leading term here is $\eta_{\text{lin}}(\alpha) = 2 \text{Re}\{\hat{\eta}_{1,0}e^{ik_1\alpha} + \hat{\eta}_{0,1}e^{ik_2\alpha}\}$, which will be a solution of the linearized problem.

Unlike [8], as noted above, we use a conformal mapping formulation [9, 14, 25] of the gravity-capillary water wave problem. This makes it possible to compute the normal velocity of the fluid from the velocity potential on the free surface via a quasi-periodic variant of the Hilbert transform. As in the periodic case, the Hilbert transform is a Fourier multiplier operator, but now acts on functions defined on a higher-dimensional torus. In a companion paper [37], we use this idea to develop a numerical method to compute the time evolution of solutions of the Euler equations from arbitrary quasi-periodic initial data. The present paper focuses on traveling waves in this framework.

We formulate the traveling wave computation as a nonlinear least-squares problem and use the Levenberg-Marquardt method to search for solutions. This approach builds on the overdetermined shooting methods developed by Wilkening *et al* [2, 3, 17, 32, 38] to compute standing waves and other time-periodic solutions. Specifically, we fix the ratio k_2/k_1 , denoted by k , and solve simultaneously for the phase speed c , the coefficient of surface tension τ , and the unknown Fourier modes $\hat{\eta}_{j_1, j_2}$ in (1.2) subject to the constraint that $\hat{\eta}_{1,0}$ and $\hat{\eta}_{0,1}$ have prescribed values. In Section 3, we discuss the merits of these bifurcation parameters over, say, prescribing τ and $\hat{\eta}_{1,0}$ and solving for $\hat{\eta}_{0,1}$ along with c and the other unknown Fourier modes. While the numerical method is general and can be used to search for solutions for any irrational k , for brevity we present results only for $k = 1/\sqrt{2}$. In future work we plan to extend our results to the case of finite-depth water waves and analyze the stability of solutions [12, 26, 35].

In Section 2, we define a quasi-periodic Hilbert transform, derive the equations of motion governing quasi-periodic traveling water waves, and summarize the main results and notation introduced in [37] on the more general spatially quasi-periodic initial value problem. In Section 3, we design a Fourier pseudo-spectral method to numerically solve the torus version of the quasi-periodic traveling wave equations. The discretization leads to an overdetermined nonlinear least-squares problem that we solve using a variant of the Levenberg-Marquardt method [31, 38]. In Section 4, we present a detailed numerical study of a two-parameter family of quasi-periodic traveling waves with $k = 1/\sqrt{2}$ and $g = 1$. In

Section 5, we summarize the results and discuss the effects of floating point arithmetic and whether solutions might exist for rational values of k . Finally, in Appendix A, we recall a theorem proved in [37] establishing sufficient conditions for an analytic function $z(w)$ to map the lower half-plane topologically onto a semi-infinite region bounded above by a parametrized curve. We also discuss conditions that ensure $1/|z_w|$ is uniformly bounded in the lower half-plane. We then study the dynamics of traveling waves in conformal space for various choices of a free parameter in the equations of motion that controls the tangential velocity of the surface parametrization. We show that the waves maintain a permanent form but generally travel at a non-uniform speed in conformal space as they evolve.

2. PRELIMINARIES

The primary goal of this paper is to study quasi-periodic traveling water waves using a conformal mapping framework. In this section, we establish notation; review the properties of the quasi-periodic Hilbert transform; discuss quasi-periodic conformal maps and complex velocity potentials; propose a synthesis of viewpoints between the Hou, Lowen-grub and Shelley formalism for evolving interfaces [18, 19] and the conformal mapping method of Dyachenko and Zakharov [9, 13, 41]; summarize the one-dimensional (1d) and torus versions of the equations of motion for the spatially quasi-periodic initial value problem [37]; discuss families of 1d quasi-periodic solutions corresponding to a single solution of the torus version of the problem; derive the equations governing traveling waves; and review the linear theory of quasi-periodic traveling waves.

2.1. Quasi-periodic functions and the Hilbert transform. A function $u(\alpha)$ is quasi-periodic if there exists a continuous, periodic function $\tilde{u}(\alpha)$ defined on the d -dimensional torus \mathbb{T}^d such that

$$(2.1) \quad u(\alpha) = \tilde{u}(k\alpha), \quad \tilde{u}(\alpha) = \sum_{j \in \mathbb{Z}^d} \hat{u}_j e^{i\langle j, \alpha \rangle}, \quad \alpha \in \mathbb{R}, \quad \alpha, k \in \mathbb{R}^d.$$

We generally assume $\tilde{u}(\alpha)$ is real analytic, which means the Fourier modes satisfy the symmetry condition $\hat{u}_{-j} = \overline{\hat{u}_j}$ and decay exponentially as $|j| \rightarrow \infty$, i.e. $|\hat{u}_j| \leq M e^{-\sigma|j|}$ for some $M, \sigma > 0$. Entries of the vector k are required to be linearly independent over \mathbb{Z} . Fixing this vector k , we define two versions of the Hilbert transform, one acting on u (the quasi-periodic version) and the other on \tilde{u} (the torus version):

$$(2.2) \quad H[u](\alpha) = \frac{1}{\pi} \text{PV} \int_{-\infty}^{\infty} \frac{u(\xi)}{\alpha - \xi} d\xi, \quad H[\tilde{u}](\alpha) = \sum_{j \in \mathbb{Z}^d} (-i) \text{sgn}(\langle j, k \rangle) \hat{u}_j e^{i\langle j, \alpha \rangle}.$$

Here $\text{sgn}(q) \in \{1, 0, -1\}$ depending on whether $q > 0$, $q = 0$ or $q < 0$, respectively. Note that the torus version of H is a Fourier multiplier on $L^2(\mathbb{T}^d)$ that depends on k . It is shown in [37] that

$$(2.3) \quad H[u](\alpha) = H[\tilde{u}](k\alpha),$$

and the most general bounded analytic function $f(w)$ in the lower half-plane whose real part agrees with u on the real axis has the form

$$(2.4) \quad f(w) = \hat{u}_0 + i\hat{v}_0 + \sum_{\langle j, k \rangle < 0} 2\hat{u}_j e^{i\langle j, k \rangle w}, \quad (w = \alpha + i\beta, \beta \leq 0),$$

where \hat{v}_0 is an arbitrary constant and the sum is over all $j \in \mathbb{Z}^d$ satisfying $\langle j, k \rangle < 0$. The imaginary part of f on the real axis is then given by $v = \hat{v}_0 - H[u]$. Similarly, given v , the most general bounded analytic function $f(w)$ in the lower half-plane whose imaginary part agrees with v on the real axis has the form (2.4) with $u = \hat{u}_0 + H[v]$, where \hat{u}_0 is an arbitrary constant. This analytic extension is quasi-periodic on slices of constant depth, i.e.

$$(2.5) \quad f(w) = \tilde{f}(k\alpha, \beta), \quad (w = \alpha + i\beta, \beta \leq 0),$$

where $\tilde{f}(\alpha, \beta) = \hat{u}_0 + i\hat{v}_0 + \sum_{\langle j, k \rangle < 0} 2[\hat{u}_j e^{-\langle j, k \rangle \beta}] e^{i\langle j, \alpha \rangle}$ is periodic in α for fixed $\beta \leq 0$. The torus version of the bounded analytic extension corresponding to $\tilde{u}(\alpha + \theta)$ is simply $\tilde{f}(\alpha + \theta, \beta)$, which has imaginary part $\tilde{v}(\alpha + \theta)$ on the real axis. As a result, the Hilbert transform commutes with the shift operator,

$$(2.6) \quad H[\tilde{u}(\cdot + \theta)](\alpha) = H[\tilde{u}](\alpha + \theta),$$

which can also be checked directly from (2.2). We also define quasi-periodic and torus versions of two projection operators,

$$(2.7) \quad P = \text{id} - P_0, \quad P_0[u] = P_0[\tilde{u}] = \hat{u}_0 = \frac{1}{(2\pi)^d} \int_{\mathbb{T}^d} \tilde{u}(\alpha) d\alpha_1 \dots d\alpha_d,$$

where $P_0[u]$ is a constant function on \mathbb{R} , $P_0[\tilde{u}]$ is a constant function on \mathbb{T}^d , and $P[u]$ has zero-mean on \mathbb{R} in the sense that its torus representation, $P[\tilde{u}]$, which satisfies $P[u](\alpha) = P[\tilde{u}](k\alpha)$, has zero mean on \mathbb{T}^d .

2.2. A quasi-periodic conformal mapping. For the general initial value problem [37], we consider a time-dependent conformal map $z(w, t)$ that maps the lower half-plane

$$(2.8) \quad \mathbb{C}^- = \{w = \alpha + i\beta : \alpha \in \mathbb{R}, \beta < 0\}$$

to the fluid domain $\Omega_f(t)$ that lies below the free surface in physical space. At each time t , we assume $z(w, t)$ extends continuously to $\overline{\mathbb{C}^-}$, and in fact is analytic on a slightly larger half-plane $\mathbb{C}_\varepsilon^- = \{w : \text{Im } w < \varepsilon\}$, where $\varepsilon > 0$ could depend on t . The free surface $\Gamma(t)$ is parametrized by

$$(2.9) \quad \zeta(\alpha, t) = \xi(\alpha, t) + i\eta(\alpha, t), \quad (\alpha \in \mathbb{R}, t \text{ fixed}), \quad \zeta = z|_{\beta=0}.$$

We assume $\alpha \mapsto \zeta(\alpha, t)$ is injective but do not assume $\Gamma(t)$ is the graph of a single-valued function of x ; an example of a spatially quasi-periodic overturning wave is computed in [37].

The conformal map is required to remain a bounded distance from the identity map in the lower half-plane. Specifically, we require that

$$(2.10) \quad |z(w, t) - w| \leq M(t) \quad (w = \alpha + i\beta, \beta \leq 0),$$

where $M(t)$ is a uniform bound that could vary in time. The Cauchy integral formula implies that $|z_w - 1| \leq M(t)/|\beta|$, so at any fixed time,

$$(2.11) \quad z_w \rightarrow 1 \quad \text{as} \quad \beta \rightarrow -\infty.$$

In this paper and its companion [37], we assume η has two spatial quasi-periods, i.e. at any time it has the form (2.1) with $d = 2$ and $k = [k_1, k_2]^T$. This is a major departure from previous work [13, 16, 27, 41], where η is periodic. Through non-dimensionalization, we may assume $k_1 = 1$ and $k_2 = k$, where k is irrational:

$$(2.12) \quad \eta(\alpha, t) = \tilde{\eta}(\alpha, k\alpha, t), \quad \tilde{\eta}(\alpha_1, \alpha_2, t) = \sum_{j_1, j_2 \in \mathbb{Z}} \hat{\eta}_{j_1, j_2}(t) e^{i(j_1 \alpha_1 + j_2 \alpha_2)}.$$

Here $\hat{\eta}_{-j_1, -j_2}(t) = \overline{\hat{\eta}_{j_1, j_2}(t)}$ since $\tilde{\eta}(\alpha_1, \alpha_2, t)$ is real-valued. Since $w \mapsto [z(w, t) - w]$ is bounded and analytic on \mathbb{C}^- and its imaginary part agrees with η on the real axis, there is a real number x_0 (possibly depending on time) such that

$$(2.13) \quad \xi(\alpha, t) = \alpha + x_0(t) + H[\eta](\alpha, t), \quad \xi_\alpha(\alpha, t) = 1 + H[\eta_\alpha](\alpha, t).$$

We use a tilde to denote the periodic functions on the torus that correspond to the quasi-periodic parts of ξ, ζ and z ,

$$(2.14) \quad \begin{aligned} \tilde{\xi}(\alpha, t) &= \alpha + \tilde{\xi}(\alpha, k\alpha, t), & \tilde{\zeta}(\alpha, t) &= \alpha + \tilde{\zeta}(\alpha, k\alpha, t), \\ z(\alpha + i\beta, t) &= (\alpha + i\beta) + \tilde{z}(\alpha, k\alpha, \beta, t), & (\beta \leq 0). \end{aligned}$$

Specifically, $\tilde{\xi} = x_0(t) + H[\tilde{\eta}]$, $\tilde{\zeta} = \tilde{\xi} + i\tilde{\eta}$, and

$$(2.15) \quad \tilde{z}(\alpha_1, \alpha_2, \beta, t) = x_0(t) + i\hat{\eta}_{0,0}(t) + \sum_{j_1+j_2k<0} \left(2i\hat{\eta}_{j_1, j_2}(t) e^{-(j_1+j_2k)\beta} \right) e^{i(j_1\alpha_1+j_2\alpha_2)}.$$

Since the modes $\hat{\eta}_{j_1, j_2}$ are assumed to decay exponentially, there is a uniform bound $M(t)$ such that $|\tilde{z}(\alpha_1, \alpha_2, \beta, t)| \leq M(t)$ for $(\alpha_1, \alpha_2) \in \mathbb{T}^2$ and $\beta \leq 0$. In [37], we show that as long as the free surface $\zeta(\alpha, t)$ does not self-intersect at a given time t , the mapping $w \mapsto z(w, t)$ is an analytic isomorphism of the lower half-plane onto the fluid region.

2.3. The complex velocity potential and equations of motion for the initial value problem. Adopting the notation of [37], let $\Phi^{\text{phys}}(x, y, t)$ denote the velocity potential in physical space and let $W^{\text{phys}}(x + iy, t) = \Phi^{\text{phys}}(x, y, t) + i\Psi^{\text{phys}}(x, y, t)$ denote the complex velocity potential, where Ψ^{phys} is the stream function. Using the conformal mapping $z(w, t)$, we pull back these functions to the lower half-plane and define

$$W(w, t) = \Phi(\alpha, \beta, t) + i\Psi(\alpha, \beta, t) = W^{\text{phys}}(z(w, t), t), \quad (w = \alpha + i\beta).$$

We also define

$$(2.16) \quad \varphi = \Phi|_{\beta=0}, \quad \psi = \Psi|_{\beta=0}.$$

We assume φ is quasi-periodic with the same quasi-periods as η ,

$$(2.17) \quad \varphi(\alpha, t) = \tilde{\varphi}(\alpha, k\alpha, t), \quad \tilde{\varphi}(\alpha_1, \alpha_2, t) = \sum_{j_1, j_2 \in \mathbb{Z}} \hat{\varphi}_{j_1, j_2}(t) e^{i(j_1\alpha_1 + j_2\alpha_2)}.$$

The fluid velocity $\nabla\Phi^{\text{phys}}(x, y, t)$ is assumed to decay to zero as $y \rightarrow -\infty$ (since we work in the lab frame). Since $dW/dw = (dW^{\text{phys}}/dz)(dz/dw)$, it follows from (2.11) that $dW/dw \rightarrow 0$ as $\beta \rightarrow -\infty$. Thus,

$$(2.18) \quad \psi_\alpha = -H[\varphi_\alpha], \quad \psi(\alpha, t) = -H[\varphi](\alpha, t).$$

Here we have assumed $P_0[\varphi] = \hat{\varphi}_{0,0}(t) = 0$ and $P_0[\psi] = \hat{\psi}_{0,0}(t) = 0$, which is allowed since Φ and Ψ can be modified by additive constants (or functions of time only) without affecting the fluid motion.

Let U and V denote the normal and tangential velocities of the curve parametrization, respectively; let $s_\alpha = |\zeta_\alpha| = (\xi_\alpha^2 + \eta_\alpha^2)^{1/2}$ denote the rate at which arclength increases as the curve $\alpha \mapsto \zeta(\alpha, t)$ is traversed; and let θ denote the tangent angle of the curve relative to the horizontal. Then

$$(2.19) \quad \zeta_\alpha = s_\alpha e^{i\theta}, \quad \zeta_t = (V + iU)e^{i\theta}.$$

Tracking a fluid particle $x_p(t) + iy_p(t) = \zeta(\alpha_p(t), t)$ on the free surface, we find that

$$\dot{x}_p = \xi_\alpha \dot{\alpha}_p + \xi_t = \Phi_x^{\text{phys}}, \quad \dot{y}_p = \eta_\alpha \dot{\alpha}_p + \eta_t = \Phi_y^{\text{phys}}.$$

Eliminating $\dot{\alpha}_p$ gives the kinematic condition

$$(2.20) \quad U = \zeta_t \cdot \hat{n} = \nabla \Phi^{\text{phys}} \cdot \hat{n},$$

where $\hat{n} = (-\eta_\alpha, \xi_\alpha)/s_\alpha$ is the outward unit normal to Γ and we have identified ζ_t with the vector (ξ_t, η_t) in \mathbb{R}^2 . The general philosophy proposed by Hou, Lowengrub and Shelley (HLS) [18, 19] is that while (2.20) constrains the normal velocity U of the curve to match that of the fluid, the tangential velocity V can be chosen arbitrarily to improve the mathematical properties of the representation or the accuracy and stability of the numerical scheme. Whereas HLS propose choosing V to keep $s_\alpha(t)$ independent of α , we interpret the work of Zakharov and Dyachenko [9, 13, 41] as choosing V to maintain a conformal representation. Briefly, since Φ^{phys} and Ψ^{phys} satisfy the Cauchy-Riemann equations,

$$(2.21) \quad -\frac{\psi_\alpha}{s_\alpha} = -\frac{\Psi_x^{\text{phys}} \xi_\alpha + \Psi_y^{\text{phys}} \eta_\alpha}{s_\alpha} = \frac{\Phi_y^{\text{phys}} \xi_\alpha - \Phi_x^{\text{phys}} \eta_\alpha}{s_\alpha} = \nabla \Phi^{\text{phys}} \cdot \hat{n} = U.$$

Assuming z_t/z_α is bounded and analytic in the lower half-plane (see Appendix ??),

$$(2.22) \quad \left. \frac{z_t}{z_\alpha} \right|_{\beta=0} = \frac{\zeta_t}{\zeta_\alpha} = \frac{V + iU}{s_\alpha} \Rightarrow \frac{V}{s_\alpha} = H\left(\frac{U}{s_\alpha}\right) + C_1 = -H\left(\frac{\psi_\alpha}{s_\alpha^2}\right) + C_1,$$

where C_1 is an arbitrary constant that we are free to choose. The tangential and normal velocities can be rotated back to obtain ξ_t and η_t via

$$(2.23) \quad \begin{pmatrix} \xi_t \\ \eta_t \end{pmatrix} = \begin{pmatrix} \xi_\alpha & -\eta_\alpha \\ \eta_\alpha & \xi_\alpha \end{pmatrix} \begin{pmatrix} V/s_\alpha \\ U/s_\alpha \end{pmatrix},$$

which can be interpreted as the real and imaginary parts of the complex multiplication $\zeta_t = (\zeta_\alpha)(\zeta_t/\zeta_\alpha)$. As explained in [37], the first equation of (2.23) is automatically satisfied if the second equation holds and ξ is reconstructed from η via (2.13), provided $x_0(t)$ satisfies

$$(2.24) \quad \frac{dx_0}{dt} = P_0 \left[\xi_\alpha \frac{V}{s_\alpha} - \eta_\alpha \frac{U}{s_\alpha} \right].$$

The equations of motion for water waves in the conformal framework may now be written

$$(2.25) \quad \begin{aligned} \xi_\alpha &= 1 + H[\eta_\alpha], & \psi &= -H[\varphi], & J &= \xi_\alpha^2 + \eta_\alpha^2, & \chi &= \frac{\psi_\alpha}{J}, \\ &\text{choose } C_1 \text{ (see below),} & & \text{compute } \frac{dx_0}{dt} \text{ in (2.24) if necessary,} & & & \\ \eta_t &= -\eta_\alpha H[\chi] - \xi_\alpha \chi + C_1 \eta_\alpha, & \kappa &= \frac{\xi_\alpha \eta_{\alpha\alpha} - \eta_\alpha \xi_{\alpha\alpha}}{J^{3/2}}, \\ \varphi_t &= P \left[\frac{\psi_\alpha^2 - \varphi_\alpha^2}{2J} - \varphi_\alpha H[\chi] + C_1 \varphi_\alpha - g\eta + \tau\kappa \right], \end{aligned}$$

where the last equation comes from the unsteady Bernoulli equation and the Laplace-Young condition for the pressure; see [37] for details.

As noted in [37], equations (2.25) can be interpreted as an evolution equation for the functions $\tilde{\zeta}(\alpha_1, \alpha_2, t)$ and $\tilde{\varphi}(\alpha_1, \alpha_2, t)$ on the torus \mathbb{T}^2 . The α -derivatives are replaced by the directional derivatives $[\partial_{\alpha_1} + k\partial_{\alpha_2}]$ and the quasi-periodic Hilbert transform is replaced

by its torus version, i.e. $H[\tilde{u}]$ in (2.2) above. The pseudo-spectral method proposed in [37] is based on this representation. A convenient choice of C_1 is

$$(2.26) \quad C_1 = \left[H \left(\frac{\tilde{\psi}_\alpha}{\tilde{f}} \right) - \frac{\tilde{\eta}_\alpha \tilde{\psi}_\alpha}{(1 + \tilde{\xi}_\alpha) \tilde{f}} \right]_{(\alpha_1, \alpha_2) = (0, 0)},$$

which causes $\tilde{\xi}(0, 0, t)$ to remain constant in time, alleviating the need to evolve $x_0(t)$ explicitly. Here $\tilde{f} = (1 + \tilde{\xi}_\alpha)^2 + \tilde{\eta}_\alpha^2$. Note that ξ_α in (2.25) is replaced by

$$(2.27) \quad \widetilde{\xi}_\alpha = 1 + \xi_\alpha$$

since the secular growth term α is not part of $\tilde{\xi}$ in (2.14). Using (2.13) and (2.14), $\tilde{\xi}$ is completely determined by $x_0(t)$ and $\tilde{\eta}$, so only these have to be evolved — the formula for $\tilde{\xi}_t$ in (2.23) is redundant as long as (2.24) is satisfied.

It is shown in [37] that solving the torus version of (2.25) yields a three-parameter family of one-dimensional solutions of the form

$$(2.28) \quad \begin{aligned} \zeta(\alpha, t; \theta_1, \theta_2, \delta) &= \alpha + \delta + \tilde{\zeta}(\theta_1 + \alpha, \theta_2 + k\alpha, t), \\ \varphi(\alpha, t; \theta_1, \theta_2) &= \tilde{\varphi}(\theta_1 + \alpha, \theta_2 + k\alpha, t), \end{aligned} \quad \begin{cases} \alpha \in \mathbb{R}, t \geq 0 \\ \theta_1, \theta_2, \delta \in \mathbb{R} \end{cases}.$$

The parameters $(\theta_1, \theta_2, \delta)$ lead to the same solution as $(0, \theta_2 - k\theta_1, 0)$ up to a spatial phase shift and α -reparametrization. Thus, every solution is equivalent to one of the form

$$(2.29) \quad \begin{aligned} \zeta(\alpha, t; 0, \theta, 0) &= \alpha + \tilde{\zeta}(\alpha, \theta + k\alpha, t), \\ \varphi(\alpha, t; 0, \theta) &= \tilde{\varphi}(\alpha, \theta + k\alpha, t) \end{aligned} \quad \alpha \in \mathbb{R}, t \geq 0, \theta \in [0, 2\pi).$$

Within this smaller family, two values of θ lead to equivalent solutions if they differ by $2\pi(n_1 k + n_2)$ for some integers n_1 and n_2 . This equivalence is due to solutions “wrapping around” the torus with a spatial shift,

$$(2.30) \quad \zeta(\alpha + 2\pi n_1, t; 0, \theta, 0) = \zeta(\alpha, t; 0, \theta + 2\pi(n_1 k + n_2), 2\pi n_1), \quad (\alpha \in [0, 2\pi), n_1 \in \mathbb{Z}).$$

Here n_2 is chosen so that $0 \leq [\theta + 2\pi(n_1 k + n_2)] < 2\pi$ and we used periodicity of $\zeta(\alpha, t; \theta_1, \theta_2, \delta)$ with respect to θ_1 and θ_2 .

It is shown in [37] that if all the waves in the family (2.29) are single-valued and have no vertical tangent lines, there is a corresponding family of solutions of the Euler equations in a standard graph-based formulation [10, 21, 40] that are quasi-periodic in physical space.

2.4. Quasi-periodic traveling water waves. We now specialize to the case of quasi-periodic traveling waves and derive the equations of motion in a conformal mapping framework. One approach (see e.g. [28] for the periodic case) is to write down the equations of motion in a graph-based representation of the surface variables $\eta^{\text{phys}}(x, t)$ and $\varphi^{\text{phys}}(x, t) = \Phi^{\text{phys}}(x, \eta(x, t), t)$ and substitute $\eta_t^{\text{phys}} = -c\eta_x^{\text{phys}}$, $\varphi_t^{\text{phys}} = -c\varphi_x^{\text{phys}}$ to solve for the initial condition of a solution of the form

$$(2.31) \quad \eta^{\text{phys}}(x, t) = \eta_0^{\text{phys}}(x - ct), \quad \varphi^{\text{phys}}(x, t) = \varphi_0^{\text{phys}}(x - ct).$$

We present below an alternative derivation of the equations in [28] that is more direct and does not assume the wave profile is single-valued. Other systems of equations have also been derived to describe traveling water waves, e.g. by Nekrasov [29, 30] and Dyachenko *et. al.* [15].

Recall the kinematic condition (2.21) that the normal velocity of the curve is given by $\zeta_t \cdot \hat{n} = U = -\psi_\alpha / s_\alpha$. Since the wave travels at constant speed c in physical space, there

is a reparametrization $\beta(\alpha, t)$ such that $\zeta(\alpha, t) = \zeta(\beta(\alpha, t), 0) + ct$. Since ζ_α is tangent to the curve, the normal velocity is simply $\zeta_t \cdot \hat{n} = (c, 0) \cdot \hat{n} = -c\eta_\alpha/s_\alpha$, where we used $\hat{n} = (-\eta_\alpha, \xi_\alpha)/s_\alpha$. We conclude that

$$(2.32) \quad \psi_\alpha = c\eta_\alpha, \quad \varphi_\alpha = H[\psi_\alpha] = cH[\eta_\alpha] = c(\xi_\alpha - 1).$$

This expresses ψ and φ (up to additive constants) in terms of η and $\xi = \alpha + x_0 + H[\eta]$, leaving only η to be determined. As in the graph-based approach of (2.31) above, it suffices to compute the initial wave profile at $t = 0$ to know the full evolution of the traveling wave under (2.25); however, the wave generally travels at a non-uniform speed in conformal space in order to travel at constant speed in physical space; see Appendix A.

The two-dimensional velocity potential $\Phi^{\text{phys}}(x, y, t)$ may be assumed to exist even if the traveling wave possesses overhanging regions that cause the graph-based representation via $\eta^{\text{phys}}(x, t)$ and $\varphi^{\text{phys}}(x, t)$ to break down. In a moving frame traveling at constant speed c along with the wave, the free surface will be a streamline. Let $\check{z} = z - ct$ denote position in the moving frame and note that the complex velocity potential picks up a background flow term, $\check{W}^{\text{phys}}(\check{z}, t) = W^{\text{phys}}(\check{z} + ct, t) - c\check{z}$, and becomes time-independent. We drop t in the notation and define $\check{W}(w) = \check{W}^{\text{phys}}(\check{z}(w))$, where $\check{z}(w) = z(w, 0)$ conformally maps the lower half-plane onto the fluid region of this stationary problem. We assume $W^{\text{phys}}(\check{z}(\alpha), 0)$ is quasi-periodic with exponentially decaying mode amplitudes, so

$$|\check{W}(w) + cw| \leq |W^{\text{phys}}(\check{z}(w), 0)| + c|\check{z}(w) - w|$$

is bounded in the lower half-plane. Since the stream function $\text{Im}\{\check{W}^{\text{phys}}(\check{z})\}$ is constant on the free surface, we may assume $\text{Im}\{\check{W}(\alpha)\} = 0$ for $\alpha \in \mathbb{R}$. The function $\text{Im}\{\check{W}(w) + cw\}$ is then bounded and harmonic in the lower half-plane and satisfies homogeneous Dirichlet boundary conditions on the real line, so it is zero [4]. Up to an additive real constant,

$$(2.33) \quad \check{W}(w) = -cw.$$

Thus, $|\check{W}\check{\Phi}^{\text{phys}}|^2 = |\check{W}'(w)/\check{z}'(w)|^2 = c^2/J$. Since the free surface is a streamline in the moving frame, the steady Bernoulli equation $(1/2)|\check{W}\check{\Phi}^{\text{phys}}|^2 + g\eta + p/\rho = C$ together with the Laplace-Young condition $p = p_0 - \rho\tau\kappa$ on the pressure gives

$$(2.34) \quad \begin{aligned} \xi_\alpha &= 1 + H[\eta_\alpha], & J &= \xi_\alpha^2 + \eta_\alpha^2, \\ \kappa &= \frac{\xi_\alpha \eta_{\alpha\alpha} - \eta_\alpha \xi_{\alpha\alpha}}{J^{3/2}}, & P \left[\frac{c^2}{2J} + g\eta - \tau\kappa \right] &= 0, \end{aligned}$$

which is the desired system of equations for η .

In the quasi-periodic traveling wave problem, we seek a solution of (2.34) of the form (2.12), except that $\tilde{\eta}$ and its Fourier modes will not depend on time. Like the initial value problem, (2.34) can be interpreted as a nonlinear system of equations for $\tilde{\eta}(\alpha_1, \alpha_2)$ defined on \mathbb{T}^2 , where the α -derivatives are replaced by $[\partial_{\alpha_1} + k\partial_{\alpha_2}]$ and the Hilbert transform is replaced by its torus version in (2.2). Without loss of generality, we assume

$$(2.35) \quad \hat{\eta}_{0,0} = 0.$$

We also assume that $\tilde{\eta}$ is an even, real function of (α_1, α_2) on \mathbb{T}^2 . Hence, in our setup, the Fourier modes of $\tilde{\eta}$ satisfy

$$(2.36) \quad \hat{\eta}_{-j_1, -j_2} = \overline{\hat{\eta}_{j_1, j_2}}, \quad \hat{\eta}_{-j_1, -j_2} = \hat{\eta}_{j_1, j_2}, \quad (j_1, j_2) \in \mathbb{Z}^2.$$

This implies that all the Fourier modes $\hat{\eta}_{j_1, j_2}$ are real, and causes $\eta(\alpha) = \tilde{\eta}(\alpha, k\alpha)$ to be even as well, which is compatible with the symmetry of (2.34). However, as in (2.28), there is a larger family of quasi-periodic traveling solutions embedded in this solution, namely

$$(2.37) \quad \eta(\alpha; \theta) = \tilde{\eta}(\alpha, \theta + k\alpha).$$

As in (2.30), two values of θ lead to equivalent solutions (up to α -reparametrization and a spatial phase shift) if they differ by $2\pi(n_1k + n_2)$ for some integers n_1 and n_2 . In general, $\eta(\alpha - \alpha_0; \theta)$ will not be an even function of α for any choice of α_0 unless $\theta = 2\pi(n_1k + n_2)$ for some integers n_1 and n_2 . In the periodic case, symmetry breaking traveling water waves have been found by Zufiria [42], though most of the literature is devoted to periodic traveling waves with even symmetry.

Equations (2.34) were derived from the requirement that their solutions travel at a constant speed in physical space. In Appendix A, we consider their evolution in conformal space under (2.25) for various choices of C_1 . The 1d waves maintain a permanent form as functions of α that travel at a generally non-uniform speed, and the torus version of the waves maintain a permanent two-dimensional form that travels through the torus in the $(1, k)$ direction at a speed that generally varies in time. A particular choice of C_1 causes $\tilde{\eta}$ and $\tilde{\varphi}$ to remain stationary in time, though it is not the choice (2.26) in which $\tilde{\xi}(0, 0, t) = 0$.

2.5. Linear theory of quasi-periodic traveling waves. Linearizing (2.34) around the trivial solution $\eta(\alpha) = 0$, we obtain,

$$(2.38) \quad c^2 H[\delta\eta_\alpha] - g\delta\eta + \tau\delta\eta_{\alpha\alpha} = 0,$$

where $\delta\eta$ denotes the variation of η . Substituting (2.12) into (2.38), we obtain a resonance relation for the Fourier modes of $\delta\eta$:

$$(2.39) \quad c^2|j_1 + j_2k| - g - \tau(j_1 + j_2k)^2 = 0, \quad (j_1, j_2) \in \mathbb{Z}^2.$$

Note that $j_1 + j_2k$, which appears in the exponent of (2.12), plays the role of k in the dispersion relation (1.1). In the numerical scheme, we assume that both of the base modes $\hat{\eta}_{1,0}$, $\hat{\eta}_{0,1}$ are nonzero. (If either is zero, there is another family of periodic solutions bifurcating from the quasi-periodic family of interest here.) Setting (j_1, j_2) to $(1, 0)$ and $(0, 1)$, respectively, gives the first-order resonance conditions

$$(2.40) \quad c^2 - g - \tau = 0, \quad c^2k - g - \tau k^2 = 0.$$

These are dimensionless equations, where the wave number k_1 of the first wave has been set to 1, and $k_2 = k_1k$. For right-moving waves, we then have $c = \sqrt{g + \tau}$ and $k = g/\tau$. Any superposition of waves with wave numbers 1 and k traveling with speed c will solve the linearized problem (2.38). We introduce the notation $c_{\text{lin}} = \sqrt{g + g/k}$ and $\tau_{\text{lin}} = g/k$ to facilitate the discussion of nonlinear effects below.

3. NUMERICAL METHOD

Equations (2.34) involve computing derivatives and Hilbert transforms of quasi-periodic functions that arise in intermediate computations. Let $f(\alpha)$ denote one of these functions, and let \tilde{f} denote the corresponding periodic function on the torus,

$$(3.1) \quad f(\alpha) = \tilde{f}(\alpha, k\alpha), \quad \tilde{f}(\alpha_1, \alpha_2) = \sum_{j_1, j_2 \in \mathbb{Z}} \hat{f}_{j_1, j_2} e^{i(j_1\alpha_1 + j_2k\alpha_2)}, \quad (\alpha_1, \alpha_2) \in \mathbb{T}^2.$$

Each \tilde{f} that arises is represented by its values on a uniform $M_1 \times M_2$ grid on the torus \mathbb{T}^2 ,

$$(3.2) \quad \tilde{f}_{m_1, m_2} = \tilde{f}(2\pi m_1/M_1, 2\pi m_2/M_2), \quad (0 \leq m_1 < M_1, 0 \leq m_2 < M_2).$$

Products, powers and quotients in (2.34) are evaluated pointwise on the grid while derivatives and the Hilbert transform are computed in Fourier space via

$$(3.3) \quad \begin{aligned} \widetilde{f}_\alpha(\alpha_1, \alpha_2) &= \sum_{j_1, j_2 \in \mathbb{Z}} i(j_1 + j_2 k) \hat{f}_{j_1, j_2} e^{i(j_1 \alpha_1 + j_2 \alpha_2)}, \\ \widetilde{H[f]}(\alpha_1, \alpha_2) &= \sum_{j_1, j_2 \in \mathbb{Z}} (-i) \operatorname{sgn}(j_1 + j_2 k) \hat{f}_{j_1, j_2} e^{i(j_1 \alpha_1 + j_2 \alpha_2)}. \end{aligned}$$

We use the ‘r2c’ version of the 2d FFTW library to rapidly compute the forward and inverse transform given by

$$(3.4) \quad \hat{f}_{j_1, j_2} = \frac{1}{M_2} \sum_{m_2=0}^{M_2-1} \left(\frac{1}{M_1} \sum_{m_1=0}^{M_1-1} \tilde{f}_{m_1, m_2} e^{-2\pi i j_1 m_1 / M_1} \right) e^{-2\pi i j_2 m_2 / M_2}, \quad \begin{pmatrix} 0 \leq j_1 \leq M_1/2 \\ -M_2/2 < j_2 \leq M_2/2 \end{pmatrix}.$$

The FFTW library actually returns the index range $0 \leq j_2 < M_2$, but we use $\hat{f}_{j_1, j_2 - M_2} = \hat{f}_{j_1, j_2}$ to de-alias the Fourier modes and map the indices $j_2 > M_2/2$ to their correct negative values. The missing entries with $-M_1/2 < j_1 < 0$ are determined implicitly by

$$(3.5) \quad \hat{f}_{-j_1, -j_2} = \overline{\hat{f}_{j_1, j_2}}.$$

When computing f_α and $H[f]$ via (3.3), the Nyquist modes with $j_1 = M_1/2$ or $j_2 = M_2/2$ are set to zero, which ensures that the ‘c2r’ transform reconstructs real-valued functions \widetilde{f}_α and $\widetilde{H[f]}$ from their Fourier modes. Further details on this pseudo-spectral representation are given in [37] in the context of timestepping the dynamic equations (2.25).

In [38], an overdetermined shooting algorithm based on the Levenberg-Marquardt method [31] was proposed for computing standing water waves accurately and efficiently. Here we adapt this method to compute quasi-periodic traveling waves instead of standing waves. We first formulate the problem in a nonlinear least-squares framework. We consider τ , c^2 (which we denote as b) and η as unknowns in (2.34) and define the residual function

$$(3.6) \quad \mathcal{R}[\tau, b, \hat{\eta}] := P \left[\frac{b}{2\tilde{f}} + g\tilde{\eta} - \tau\tilde{\kappa} \right].$$

Here, $\hat{\eta}$ represents the Fourier modes of η , which are assumed real via (2.36); J and κ depend on η through the auxiliary equations of (2.34); and a tilde indicates that the function is represented on the torus, \mathbb{T}^2 , as in (3.1). We also define the objective function

$$(3.7) \quad \mathcal{F}[\tau, b, \hat{\eta}] := \frac{1}{8\pi^2} \int_{\mathbb{T}^2} \mathcal{R}^2[\tau, b, \hat{\eta}] d\alpha_1 d\alpha_2.$$

Note that solving (2.34) is equivalent to finding a zero of the objective function $\mathcal{F}[\tau, b, \hat{\eta}]$. The parameter k in (3.1) is taken to be a fixed, irrational number when searching for zeros of \mathcal{F} .

In the numerical computation, we truncate the problem to finite dimensions by varying only the leading Fourier modes $\hat{\eta}_{j_1, j_2}$ with $0 \leq |j_1|, |j_2| \leq N/2$. We evaluate the residual \mathcal{R} (and compute the Fourier transforms) on an $M \times M$ grid, where $M > N$. The resulting nonlinear least squares problem is overdetermined because we zero-pad the Fourier modes

$\hat{\eta}_{j_1, j_2}$ when $|j_1|$ or $|j_2|$ is larger than $N/2$. Assuming the $\hat{\eta}_{j_1, j_2}$ are real (i.e. that η is even) also reduces the number of unknowns relative to the number of equations, which are enumerated by the M^2 gridpoints without exploiting symmetry. According to the linear theory of Section 2.5, we fix the two base Fourier modes $\hat{\eta}_{1,0}$ and $\hat{\eta}_{0,1}$ at nonzero amplitudes; these amplitudes are chosen independently. It might seem more natural to prescribe τ and $\hat{\eta}_{1,0}$ and solve for $\hat{\eta}_{0,1}$ along with b and the other unknown Fourier modes of η . However, linearization about the flat state leads to $\partial \mathcal{R} / \partial \tau = 0$ (since $\eta \equiv 0 \Rightarrow \kappa \equiv 0$). This prevents the use of the implicit function theorem to solve the system in terms of τ and $\hat{\eta}_{1,0}$ and would also cause difficulties for the numerical solver. Note that by (2.40) above, to linear order we have $\tau = g/k$ and $c = \sqrt{g + g/k}$. Variations in τ and c enter at higher order when the two amplitude parameters $\hat{\eta}_{1,0}$ and $\hat{\eta}_{0,1}$ are perturbed from 0, as shown below.

The Levenberg-Marquardt solver requires a linear ordering of the unknowns. We enumerate the $\hat{\eta}_{j_1, j_2}$ so that lower-frequency modes appear first. As the “shell index” s ranges from 1 to $N/2$, we enumerate all the index pairs (j_1, j_2) with $\max(|j_1|, |j_2|) = s$ before increasing s . Within shell s , we proceed clockwise, along straight lines through the lattice, from $(0, s)$ to (s, s) to $(s, -s)$ to $(1, -s)$. The other Fourier modes are known from (2.35) and (2.36). Shell s contains $4s$ index pairs, so the total number of independent modes $\hat{\eta}_{j_1, j_2}$ with $\max(|j_1|, |j_2|) \leq N/2$ is $\sum_{s=1}^{N/2} 4s = N(N/2 + 1)$. We replace $\hat{\eta}_{1,0}$ by τ and $\hat{\eta}_{0,1}$ by b in the list of unknowns to avoid additional shuffling of the variables when the prescribed base modes are removed from the list. Eventually there are $N(N/2 + 1)$ parameters to compute:

$$p_1 = \tau, \quad p_2 = \hat{\eta}_{1,1}, \quad p_3 = b, \quad p_4 = \hat{\eta}_{1,-1}, \quad p_5 = \hat{\eta}_{0,2}, \quad \dots, \quad p_{N(N/2+1)} = \hat{\eta}_{1,-N/2}.$$

The objective function \mathcal{F} is evaluated numerically by the trapezoidal rule approximation over \mathbb{T}^2 , which is spectrally accurate:

$$(3.9) \quad \begin{aligned} f(p) &= \frac{1}{2} r(p)^T r(p) \approx \mathcal{F}[\tau, b, \hat{\eta}], \\ r_m(p) &= \mathcal{R}[\tau, b, \eta](\alpha_{m_1}, \alpha_{m_2})/M, \end{aligned} \quad \begin{pmatrix} m = 1 + m_1 + Mm_2 \\ \alpha_{m_i} = 2\pi m_i/M \end{pmatrix}, \quad 0 \leq m_i < M.$$

The parameters p_j are chosen to minimize $f(p)$ using the Levenberg-Marquardt method [31, 38]. The method requires a Jacobian matrix $(\partial r_m / \partial p_j)_{mj}$, which we compute by solving the following variational equations:

$$(3.10) \quad \begin{aligned} \delta \xi_\alpha &= H[\delta \eta_\alpha], & \delta J &= 2(\xi_\alpha \delta \xi_\alpha + \eta_\alpha \delta \eta_\alpha), \\ \delta \kappa &= -\frac{3}{2} \kappa \frac{\delta J}{J} + \frac{1}{J^{3/2}} \left(\delta \xi_\alpha \eta_{\alpha\alpha} + \xi_\alpha \delta \eta_{\alpha\alpha} - \delta \eta_\alpha \xi_{\alpha\alpha} - \eta_\alpha \delta \xi_{\alpha\alpha} \right), \\ \delta \mathcal{R}[\tau, b, \hat{\eta}] &= P \left[\frac{\delta b}{2\tilde{J}} - \frac{1}{2\tilde{J}^2} b \tilde{\delta J} + g \tilde{\delta \eta} - \delta \tau \tilde{\kappa} - \tau \tilde{\delta \kappa} \right]. \end{aligned}$$

We then have $\frac{\partial r_m}{\partial p_j} = \delta \mathcal{R}[\tau, b, \hat{\eta}](\alpha_{m_1}, \alpha_{m_2})$, where $m = 1 + m_1 + Mm_2$ and the j th column of the Jacobian corresponds to setting the perturbation $\delta \tau$, δb or $\delta \hat{\eta}_{j_1, j_2}$ corresponding to p_j in (3.8) to 1 and the others to 0.

Like Newton’s method, the Levenberg-Marquardt method generates a sequence of approximate solutions $p^{(0)}$, $p^{(1)}$, etc., which terminate when the residual drops below the desired tolerance or fails to decrease sufficiently. If no other solutions have been computed,

we use the solution of the linearized problem as an initial guess:

$$(3.11) \quad \begin{aligned} \eta^{(0)}(\alpha) &= \hat{\eta}_{1,0}(e^{i\alpha} + e^{-i\alpha}) + \hat{\eta}_{0,1}(e^{ik\alpha} + e^{-ik\alpha}), \\ \tau^{(0)} &= \tau_{\text{lin}} = g/k, \quad b^{(0)} = c_{\text{lin}}^2 = g + g/k. \end{aligned}$$

After computing two small-amplitude solutions, we use numerical continuation to increase the amplitude beyond the applicability of linear theory. In the present work, we hold the ratio $\gamma = \hat{\eta}_{1,0}/\hat{\eta}_{0,1}$ constant to explore one-dimensional slices (or paths) through the two-dimensional family of quasi-periodic traveling waves. We find that linear extrapolation from the previous two solutions on a path works well as the starting guess for the next Levenberg-Marquardt solve. Details of our Levenberg-Marquardt implementation, including stopping criteria and a strategy for delaying the re-computation of the Jacobian, are given in [38].

4. NUMERICAL RESULTS

We now present a detailed numerical study of solutions of (2.34) with $k = 1/\sqrt{2}$ and $g = 1$ on three continuation paths corresponding to $\gamma \in \{5, 1, 0.2\}$, where $\gamma = \hat{\eta}_{1,0}/\hat{\eta}_{0,1}$ is the amplitude ratio of the prescribed base modes. In each case, we vary the larger of $\hat{\eta}_{1,0}$ and $\hat{\eta}_{0,1}$ from 0.001 to 0.01 in increments of 0.001. The initial guess for the first two solutions on each path are obtained using the linear approximation (3.11), which by (3.8) corresponds to

$$(4.1) \quad p_1^{(0)} = \tau^{(0)} = \sqrt{2}, \quad p_3^{(0)} = b^{(0)} = 1 + \sqrt{2}, \quad p_j^{(0)} = 0, \quad j \notin \{1, 3\}.$$

As noted already, the amplitudes $\hat{\eta}_{1,0}$ and $\hat{\eta}_{0,1}$ are prescribed — they are not included among the unknowns. The initial guess for the remaining 8 solutions on each continuation path are obtained from linear extrapolation from the previous two computed solutions. In all cases, we use $M = 60$ for the grid size and $N = 48$ for the Fourier cutoff in each dimension.

Figure 1 shows the initial conditions η and φ for the last solution on each continuation path (with $\max\{\hat{\eta}_{1,0}, \hat{\eta}_{0,1}\} = 0.01$). Panels (a), (b) and (c) correspond to $\gamma = 5, 1$, and 0.2 , respectively. The solution in all three cases is quasi-periodic, i.e. η and φ never exactly repeat themselves; we plot the solution from $x = 0$ to $x = 36\pi$ as a representative snapshot. For these three solutions, the objective function f in (3.9) was minimized to 6.05×10^{-28} , 9.28×10^{-28} and 4.25×10^{-28} , respectively, with similar or smaller values for lower-amplitude solutions on each path. The number of Jacobian evaluations in the Levenberg-Marquardt method for each of the 30 solutions computed on these paths never exceeded 5, and is typically 3 or 4. In our computations, η and φ are represented by $\tilde{\eta}(\alpha_1, \alpha_2)$ and $\tilde{\varphi}(\alpha_1, \alpha_2)$, which are defined on the torus \mathbb{T}^2 . In Figure 2, we show contour plots of $\tilde{\eta}(\alpha_1, \alpha_2)$ and $\tilde{\varphi}(\alpha_1, \alpha_2)$ corresponding to the final solution on each path. Following the dashed lines through \mathbb{T}^2 in Figure 2 leads to the plots in Figure 1. By construction in (2.36), $\tilde{\eta}(-\alpha) = \tilde{\eta}(\alpha)$ while $\tilde{\varphi}(-\alpha) = -\tilde{\varphi}(\alpha)$.

The amplitude ratio, $\gamma := \hat{\eta}_{1,0}/\hat{\eta}_{0,1}$, determines the bulk shape of the solution. If $\gamma \gg 1$, the wave with wave number 1 will be dominant; if $\gamma \ll 1$, the wave with wave number $k = 2^{-1/2}$ will be dominant; and if γ is close to 1, both waves together will be dominant over higher-frequency Fourier modes (at least in the regime we study here). This is demonstrated with $\gamma = 5, 1$ and 0.2 in panels (a), (b) and (c) of Figure 1. Panels (a) and (c) show a clear

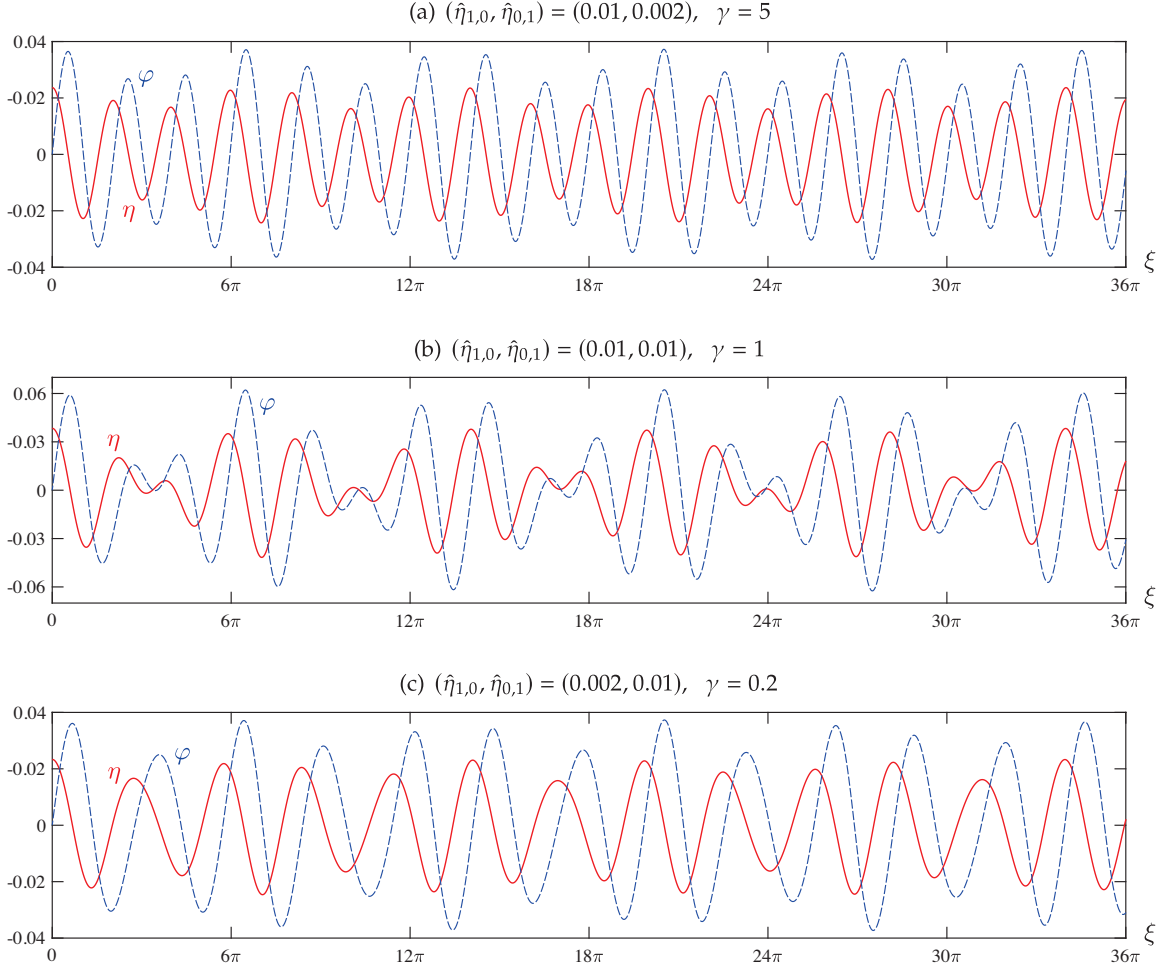


FIGURE 1. Spatially quasi-periodic traveling solutions in the lab frame at $t = 0$. The wave height $\eta(\alpha)$ (solid red line) and velocity potential $\varphi(\alpha)$ (dashed blue line) are plotted parametrically against $\xi(\alpha)$ to show the wave in physical space.

dominant mode with visible variations in the amplitude. The oscillations are faster in panel (a) than in (c) since $1 > k \approx 0.707$. By contrast, in panel (b), there is no single dominant wavelength.

This can also be understood from the plots in Figure 2. In case (a), $\gamma \gg 1$ and the contour lines of $\tilde{\eta}$ and $\tilde{\varphi}$ are perturbations of sinusoidal waves depending only on α_1 . The unperturbed waves would have vertical contour lines. The α_2 -dependence of the perturbation causes local extrema to form at the crest and trough. As a result, the contour lines join to form closed curves that are elongated vertically since the dominant variation is in the α_1 direction. Case (c) is similar, but the contour lines are elongated horizontally since the dominant variation is in the α_2 direction. Following the dashed lines in Figure 2, a cycle of α_1 is completed before a cycle of α_2 (since $k < 1$). In case (a), a cycle of α_1 traverses the dominant variation of $\tilde{\eta}$ and $\tilde{\varphi}$ on the torus, whereas in case (c), this is true of α_2 . So the waves in Figure 1 appear to oscillate faster in case (a) than case (c). In the intermediate case (b) with $\gamma = 1$, the contour lines of the crests and troughs are nearly circular, but not perfectly round. The amplitude of the waves in Figure 1 are largest when the dashed lines

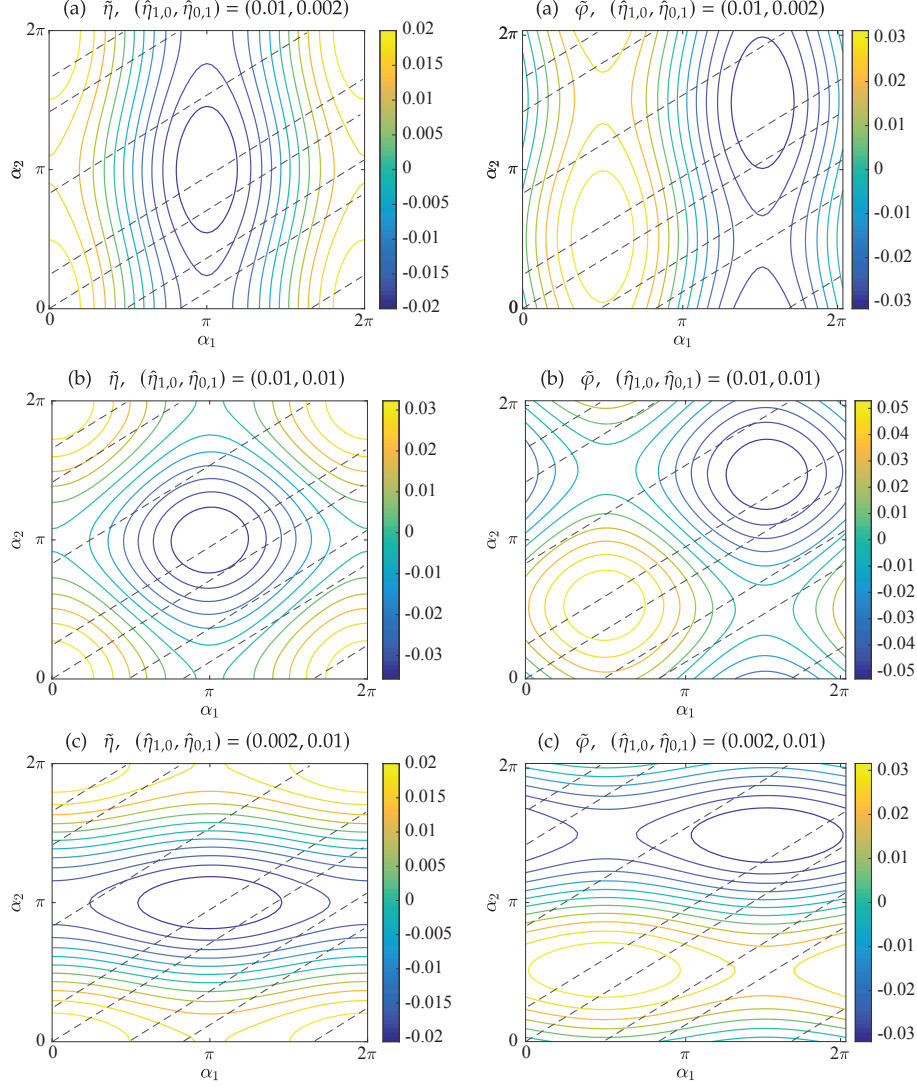


FIGURE 2. Contour plots of $\tilde{\eta}$ and $\tilde{\varphi}$ on \mathbb{T}^2 . The dashed lines show $(\alpha, k\alpha)$ and its periodic images with $0 \leq \alpha \leq 10\pi$ and $k = 1/\sqrt{2}$. Evaluating $\tilde{\eta}$ and $\tilde{\varphi}$ at these points gives η and φ in (2.12) and (2.17).

in Figure 2 pass near the extrema of $\tilde{\eta}$ and $\tilde{\varphi}$, and are smallest when the dashed lines pass near the zero level sets of $\tilde{\eta}$ and $\tilde{\varphi}$. If the slope of the dashed lines were closer to 1 and the functions $\tilde{\eta}$ and $\tilde{\varphi}$ were to remain qualitatively similar to the results of panel (b) of Figure 2, the waves would have a beating pattern with many cycles with larger amplitude followed by many cycles with smaller amplitude. The former would occur when the dashed lines pass near the diagonal from $(0, 0)$ to $(2\pi, 2\pi)$, which passes over the peaks and troughs of $\tilde{\eta}$ and $\tilde{\varphi}$, while the latter would occur when the dashed lines pass near the lines connecting $(\pi, 0)$ to $(2\pi, \pi)$ and $(0, \pi)$ to $(\pi, 2\pi)$, where $\tilde{\eta}$ and $\tilde{\varphi}$ are close to zero. The dashed lines would linger in each regime over many cycles if k were close to 1.

In Figure 3, we plot the time evolution of $\zeta(\alpha, t)$ in the lab frame from $t = 0$ to $t = 3$ using the timestepping algorithm described in [37]. The initial conditions, plotted with thick blue lines, are those of the traveling waves computed in Figures 1 and 2 above. The grey curves

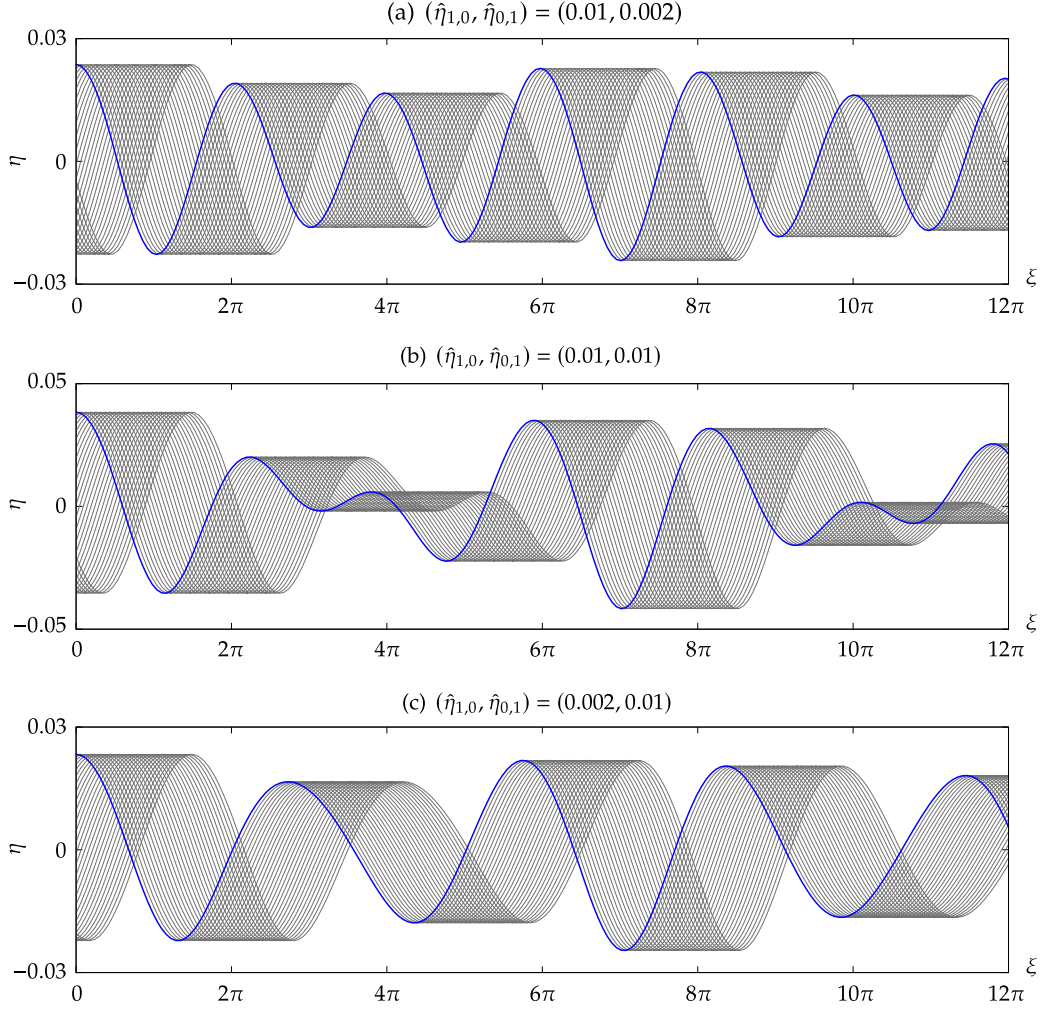


FIGURE 3. Time evolution of the traveling wave profiles, $\zeta(\alpha, t)$, from $t = 0$ to $t = 3$ in the lab frame. The thick blue lines correspond to the initial conditions.

give snapshots of the solution at uniformly sampled times with $\Delta t = 0.1$. The solutions are plotted over the representative interval $0 \leq x \leq 12\pi$, though they extend in both directions to $\pm\infty$ without exactly repeating. Note that the solutions appear to propagate to the right at constant speed without changing shape. Our next goal is to verify this quantitatively to confirm that the quasi-periodic solutions we obtained by minimizing the objective function (3.9) are indeed traveling waves under the evolution equations (2.25).

Quantitative comparison requires an “exact” solution, which we take to be the numerically computed traveling wave, spatially shifted according to the exact time evolution derived in Corollary A.5 of Appendix A. In more detail, minimizing the objective function (3.9) gives the torus version of the traveling wave profile $\tilde{\eta}_0(\alpha_1, \alpha_2)$, the surface tension τ , and the wave speed c such that $(\hat{\eta}_0)_{1,0}$ and $(\hat{\eta}_0)_{0,1}$ have prescribed values at $t = 0$. We then compute $\xi_0 = H[\tilde{\eta}_0]$ and $\tilde{\varphi}_0 = c\xi_0$, which are odd functions of $\alpha = (\alpha_1, \alpha_2)$ since $\tilde{\eta}$ is even. From Corollary A.5, the time evolution of the traveling wave with these initial conditions

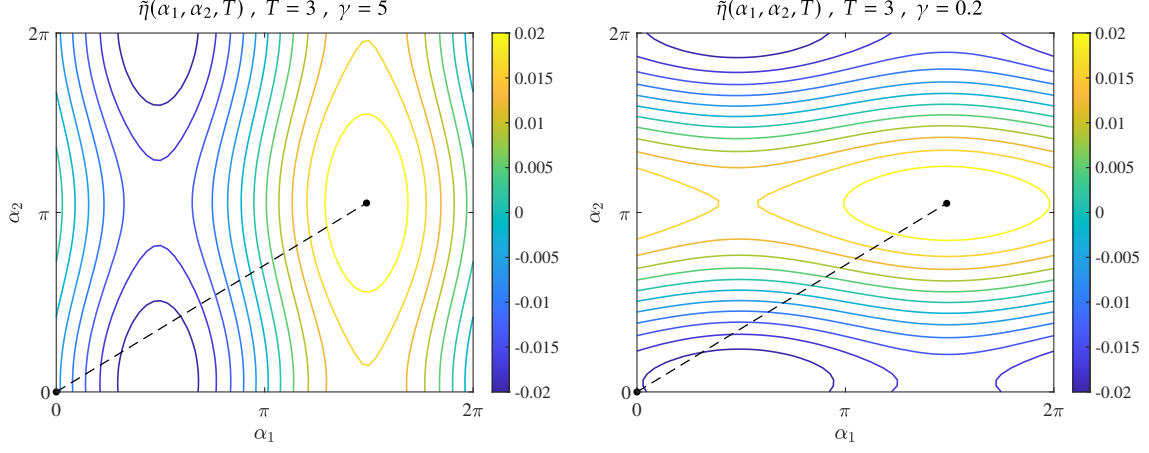


FIGURE 4. Contour plots of the numerical solution $\tilde{\eta}(\alpha_1, \alpha_2, T)$ on the torus corresponding to the quasi-periodic solutions $\eta(\alpha, t)$ of panels (a) and (c) of Figure 3 at the final time shown, $t = T = 3$. The dashed lines show the trajectory of the wave crest from $t = 0$ to $t = T$.

under the torus version of (2.25) and (2.26) is given by

$$(4.2) \quad \begin{aligned} \tilde{\eta}_{\text{exact}}(\alpha_1, \alpha_2, t) &= \tilde{\eta}_0(\alpha_1 - \alpha_0(t), \alpha_2 - k\alpha_0(t)), \\ \tilde{\varphi}_{\text{exact}}(\alpha_1, \alpha_2, t) &= \tilde{\varphi}_0(\alpha_1 - \alpha_0(t), \alpha_2 - k\alpha_0(t)), \end{aligned}$$

where $\alpha_0(t) = ct - \mathcal{A}(-ct, -kct)$ and $\mathcal{A}(x_1, x_2)$ is a periodic function on \mathbb{T}^2 defined implicitly by (A.12) below. We see in (4.2) that the waves do not change shape as they move through the torus along the characteristic direction $(1, k)$, but the traveling speed $\alpha'_0(t)$ in conformal space varies in time in order to maintain $\tilde{\xi}(0, 0, t) = 0$ via (2.26). By Corollary A.5, the exact reconstruction of $\tilde{\xi}_{\text{exact}}$ from $\tilde{\eta}_{\text{exact}}$ is

$$(4.3) \quad \tilde{\xi}_{\text{exact}}(\alpha_1, \alpha_2, t) = \tilde{\xi}_0(\alpha_1 - \alpha_0(t), \alpha_2 - k\alpha_0(t)) + \delta_0(t),$$

where $\delta_0(t) = ct - \alpha_0(t) = \mathcal{A}(-ct, -kct)$ measures the deviation in position from traveling at the constant speed ct in conformal space. The defining property (A.12) of $\mathcal{A}(x_1, x_2)$ ensures that $\tilde{\xi}_{\text{exact}}(0, 0, t) = 0$.

Figure 4 shows contour plots of the torus version of the $\gamma = 5$ and $\gamma = 0.2$ solutions shown in panels (a) and (c) of Figure 3 at the final time computed, $T = 3$. A similar plot of the $\gamma = 1$ solution is given in [37]. The dashed lines show the trajectory from $t = 0$ to $t = T$ of the wave crest that begins at $(0, 0)$ and continues along the path $\alpha_1 = \alpha_0(t)$, $\alpha_2 = k\alpha_0(t)$ through the torus in (4.2). The following table gives the phase speed, c , surface tension, τ , translational shift in conformal space at the final time computed, $\alpha_0(T)$, and deviation from steady motion in conformal space, $\delta_0(T)$, for these three finite-amplitude solutions (recall that $\max\{\hat{\eta}_{1,0}, \hat{\eta}_{0,1}\} = 0.01$ and $\hat{\eta}_{1,0}/\hat{\eta}_{0,1} = \gamma$) as well as for the zero-amplitude limit:

	$\gamma = 5$	$\gamma = 1$	$\gamma = 0.2$	linear theory	
c	1.552 175	1.552 197	1.553 743	$c_{\text{lin}} = 1.553 774$	
τ	1.409 665	1.410 902	1.415 342	$\tau_{\text{lin}} = 1.414 214$	
$\alpha_0(T)$	4.677 416	4.681 174	4.668 757	$c_{\text{lin}}T = 4.661 322$	
$\delta_0(T)$	-0.020 890	-0.024 583	-0.007 527	0	$(T = 3)$

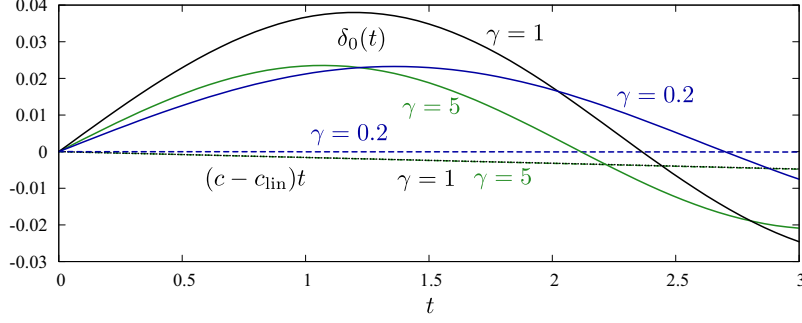


FIGURE 5. Plots of $\delta_0(t) = ct - \alpha_0(t)$ in (4.2) and $(c - c_{\text{lin}})t$ for the solutions of Figure 3.

In Figure 5, we plot $\delta_0(t)$ for $0 \leq t \leq T$ (solid lines) along with $(c - c_{\text{lin}})t$ (dashed and dotted lines) for the three finite-amplitude solutions in this table. Writing $\alpha_0(t) = c_{\text{lin}}t + [(c - c_{\text{lin}})t - \delta_0(t)]$, we see that the deviation of $\alpha_0(t)$ from linear theory over this time interval is due mostly to fluctuations in $\delta_0(t)$ rather than the steady drift $(c - c_{\text{lin}})t$ due to the change in phase speed c of the finite-amplitude wave.

Computing the exact solution (4.2) requires evaluating $\delta_0(t) = \mathcal{A}(-ct, -kct)$. We use Newton's method to solve the implicit equation (A.12) for $\mathcal{A}(x_1, x_2)$ at each point of a uniform $M \times M$ grid, with M as in Section 3. We then use FFTW to compute the 2d Fourier representation of $\mathcal{A}(x_1, x_2)$, which is used to quickly evaluate the function at any point. It would also have been easy to compute $\mathcal{A}(-ct, -kct)$ directly by Newton's method, but the Fourier approach is also very fast and gives more information about the function $\mathcal{A}(x_1, x_2)$. In particular, the modes decay to machine roundoff on the grid, corroborating the assertion in [37] that \mathcal{A} is real analytic. We use the exact solution to compute the error in timestepping (2.25) and (2.26) from $t = 0$ to $t = T$,

$$\text{err} = \sqrt{\|\tilde{\eta} - \tilde{\eta}_{\text{exact}}\|^2 + \|\tilde{\varphi} - \tilde{\varphi}_{\text{exact}}\|^2}, \quad \|\tilde{\eta}\|^2 = \frac{1}{M_1 M_2} \sum_{m_1, m_2} \tilde{\eta} \left(\frac{2\pi m_1}{M_1}, \frac{2\pi m_2}{M_2}, T \right)^2.$$

A detailed convergence study is given in [37] to compare the accuracy and efficiency of the Runge-Kutta and exponential time differencing schemes proposed in that paper using the $\gamma = 1$ traveling solution above as a test case. Here we report the errors for all three waves plotted in Figure 3

	$\gamma = 5$	$\gamma = 1$	$\gamma = 0.2$
err	1.04×10^{-16}	1.16×10^{-16}	7.38×10^{-17}

using the simplest timestepping method proposed in [37] to solve (2.25), namely a 5th order explicit Runge-Kutta method using 900 uniform steps from $t = 0$ to $t = 3$. These errors appear to mostly be due to roundoff error in floating-point arithmetic, validating the accuracy of both the timestepping algorithm of [37] and the traveling wave solver of Section 3, which was taken as the exact solution. Evolving the solutions to compute these errors took less than a second on a laptop (with $M^2 = 3600$ gridpoints and 900 timesteps), while computing the traveling waves via the Levenberg-Marquardt method took 30–40 seconds on a laptop and only 3 seconds on a server (Intel Xeon Gold 6136, 3GHz) running on 12 threads (with $M^2 = 3600$ gridpoints and $N(N/2 + 1) = 1200$ unknowns).

Next we examine the behavior of the Fourier modes that make up these solutions. Figure 6 shows two-dimensional plots of the Fourier modes $\hat{\eta}_{j_1, j_2}$ for the 3 cases above,

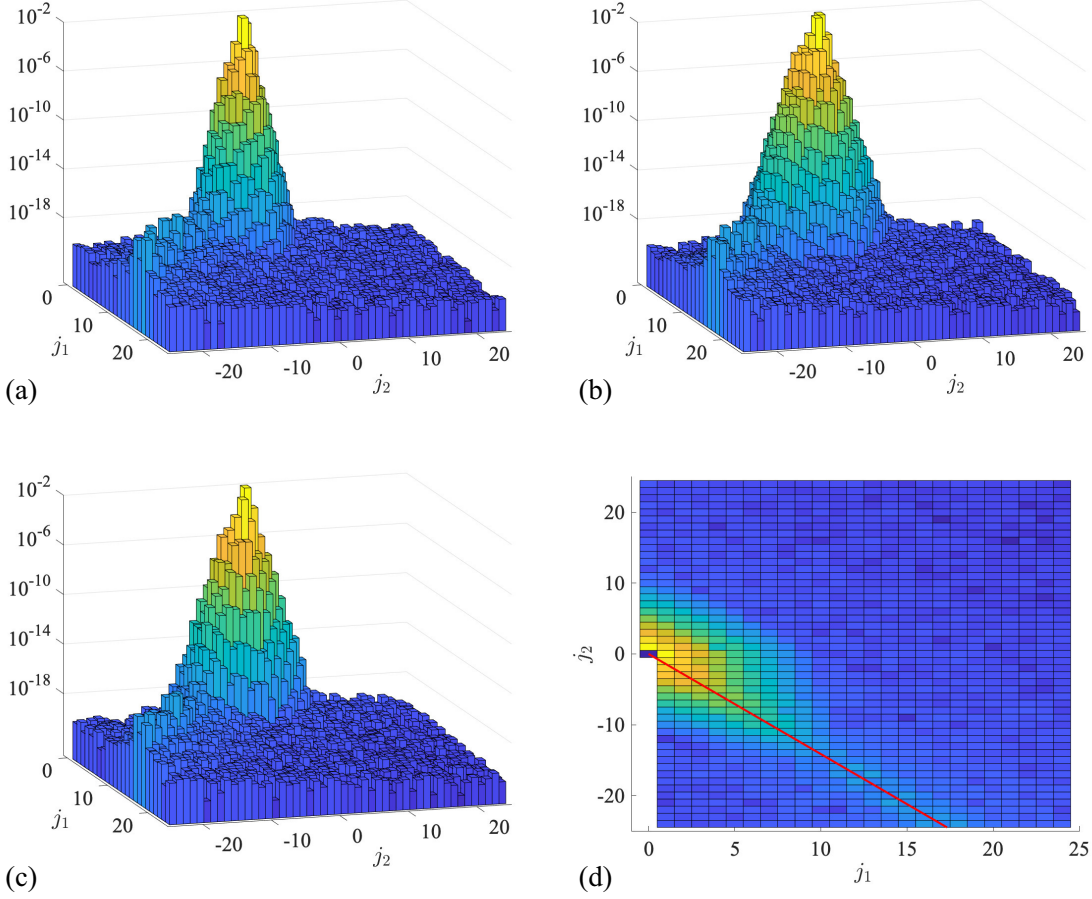


FIGURE 6. Two-dimensional Fourier modes of $\hat{\eta}$ for the $k = 1/\sqrt{2}$ solutions plotted in Figures 1 and 2. (a) $\gamma = 5$. (b,d) $\gamma = 1$. (c) $\gamma = 0.2$. In all three cases, the modes decay visibly slower along the line $j_1 + j_2 k = 0$, indicating the presence of resonant mode interactions.

with $\gamma \in \{5, 1, 0.2\}$ and $\max\{\hat{\eta}_{1,0}, \hat{\eta}_{0,1}\} = 0.01$. Only the prescribed modes and the modes that were optimized by the solver (see (3.8)) are plotted, which have indices in the range $0 \leq j_1 \leq N/2$ and $-N/2 \leq j_2 \leq N/2$, excluding $j_2 \leq 0$ when $j_1 = 0$. The other modes are determined by the symmetry of (2.36) and by zero-padding $\hat{\eta}_{j_1, j_2} = 0$ if $N/2 < j_1 \leq M$ or $N/2 < |j_2| \leq M$. We used $N = 48$ and $M = 60$ in all 3 calculations. One can see that the fixed Fourier modes $\hat{\eta}_{1,0}$ and $\hat{\eta}_{0,1}$ are the two highest-amplitude modes in all three cases. In this sense, our solutions of the nonlinear problem (2.34) are small-amplitude perturbations of (3.11). However, there are many active Fourier modes, so these solutions are well outside of the linear regime. Carrying out a weakly nonlinear Stokes expansion to high enough order to accurately predict all these modes would be difficult, especially considering the degeneracies that arise already in the periodic Wilton ripple problem [35, 36].

In panels (a), (b) and (c) of Figure 6, the modes appear to decay more slowly in one direction than in other directions. This is seen more clearly when viewed from above, as shown in panel (d) for the case of $\gamma = 1$. (The other two cases are similar). The direction along which the modes decay less rapidly appears to coincide with the line

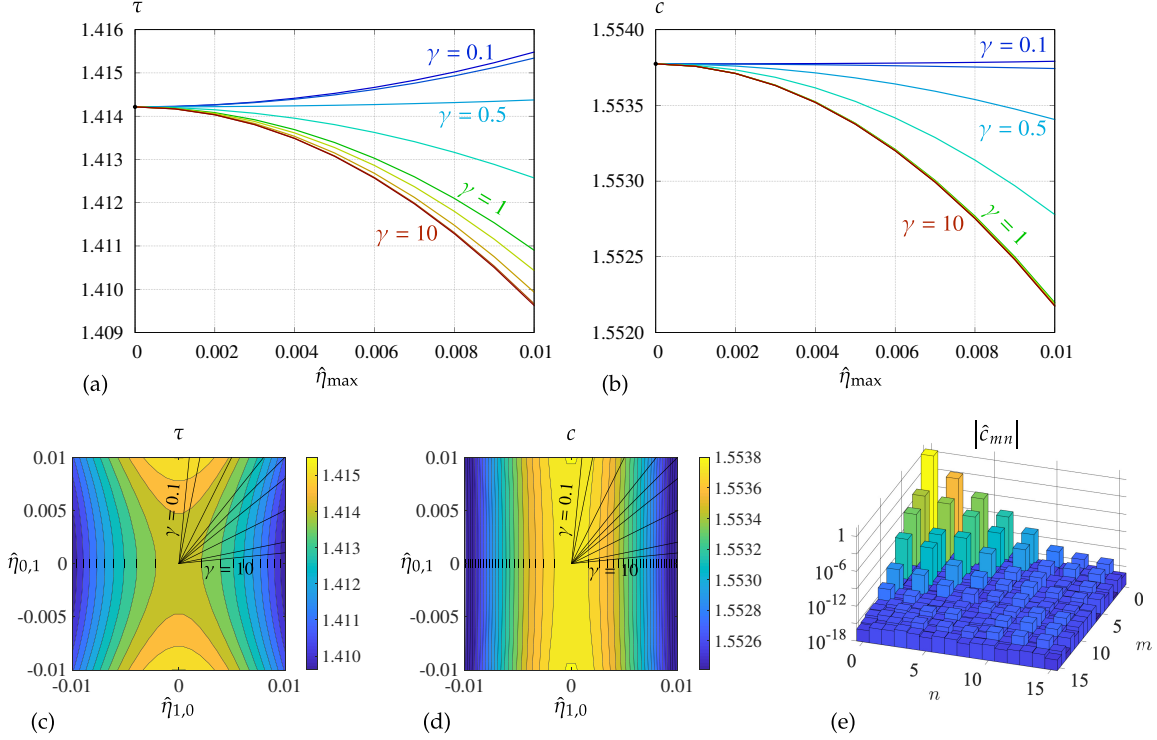


FIGURE 7. Dependence of τ and c on $\hat{\eta}_{1,0}$ and $\hat{\eta}_{0,1}$. (a,b) Plots of τ and c versus $\hat{\eta}_{\max} = \max(\hat{\eta}_{1,0}, \hat{\eta}_{0,1})$ holding $\gamma = \hat{\eta}_{1,0}/\hat{\eta}_{0,1}$ fixed. (c,d) Contour plots of τ and c and the rays of constant γ corresponding to (a,b). (e) Mode amplitudes of a 2d Chebyshev expansion of $c(\hat{\eta}_{1,0}, \hat{\eta}_{0,1})$ over the rectangle $-0.01 \leq \hat{\eta}_{1,0}, \hat{\eta}_{0,1} \leq 0.01$.

$\{(j_1, j_2) : j_1 + j_2 k = 0\}$, which is plotted in red. A partial explanation is that when $j_1 + j_2 k$ is close to zero, the corresponding modes $e^{i(j_1 + j_2 k)\alpha}$ in the expansion of $\eta(\alpha)$ in (2.12) have very long wavelength. Slowly varying perturbations lead to small changes in the residual of the water wave equations, so these modes are not strongly controlled by the governing equations (2.34). We believe this would lead to a small divisor problem [20] that would complicate a rigorous proof of existence of quasi-periodic traveling water waves.

Next we show that τ and c depend nonlinearly on the amplitude of the Fourier modes $\hat{\eta}_{1,0}$ and $\hat{\eta}_{0,1}$. Panels (a) and (b) of Figure 7 show plots of τ and c versus $\hat{\eta}_{\max} := \max(\hat{\eta}_{1,0}, \hat{\eta}_{0,1})$ for 9 values of $\gamma = \hat{\eta}_{1,0}/\hat{\eta}_{0,1}$, namely $\gamma = 0.1, 0.2, 0.5, 0.8, 1, 1.25, 2, 5, 10$. On each curve, $\hat{\eta}_{\max}$ varies from 0 to 0.01 in increments of 0.001. At small amplitude, linear theory predicts $\tau = g/k = 1.41421$ and $c = \sqrt{g(1 + 1/k)} = 1.55377$. This is represented by the black marker at $\hat{\eta}_{\max} = 0$ in each plot. For each value of γ , the curves τ and c are seen to have zero slope at $\hat{\eta}_{\max} = 0$, and can be concave up or concave down depending on γ . This can be understood from the contour plots of panels (c) and (d). Both τ and c appear to be even functions of $\hat{\eta}_{1,0}$ and $\hat{\eta}_{0,1}$ when the other is held constant. Both plots have a saddle point at the origin, are concave down in the $\hat{\eta}_{1,0}$ direction holding $\hat{\eta}_{0,1}$ fixed, and are concave up in the $\hat{\eta}_{0,1}$ direction holding $\hat{\eta}_{1,0}$ fixed. The solid lines in the first quadrant of these plots are the slices corresponding to the values of γ plotted in panels (a) and (b). The concavity of the 1d plots depends on how these lines intersect the saddle in the 2d plots.

The contour plots of panels (c) and (d) of Figure 7 were made by solving (2.34) with $(\hat{\eta}_{1,0}, \hat{\eta}_{0,1})$ ranging over a uniform 26×26 grid on the square $[-0.01, 0.01] \times [-0.01, 0.01]$. Using an even number of gridpoints avoids the degenerate case where $\hat{\eta}_{1,0}$ or $\hat{\eta}_{0,1}$ is zero. At those values, the two-dimensional family of quasi-periodic solutions meets a sheet of periodic solutions where τ or c becomes a free parameter. Alternative techniques would be needed in these degenerate cases to determine the value of τ or c from which a periodic traveling wave in the nonlinear regime bifurcates to a quasi-periodic wave. In panel (e), we plot the magnitude of the Chebyshev coefficients in the expansion

$$(4.4) \quad c(\hat{\eta}_{1,0}, \hat{\eta}_{0,1}) = \sum_{m=0}^{15} \sum_{n=0}^{15} \hat{c}_{mn} T_m(100\hat{\eta}_{1,0}) T_n(100\hat{\eta}_{0,1}), \quad -0.01 \leq \hat{\eta}_{1,0}, \hat{\eta}_{0,1} \leq 0.01.$$

This was done by evaluating c on a cartesian product of two 16-point Chebyshev-Lobatto grids over $[-0.01, 0.01]$ and using the one-dimensional Fast Fourier Transform in each direction to compute the Chebyshev modes. We see that the modes decay to machine precision by the time $m + n \geq 10$ or so, and only even modes m and n are active. The plot for $|\hat{c}_{mn}|$ is very similar, so we omit it. These plots confirm the visual observation from the contour plots that τ and c are even functions of $\hat{\eta}_{1,0}$ and $\hat{\eta}_{0,1}$ when the other is held constant. In summary, over the range $-0.01 \leq \hat{\eta}_{1,0}, \hat{\eta}_{0,1} \leq 0.01$ considered here, τ and c show interesting nonlinear effects that would be difficult to model using weakly nonlinear theory since polynomials of degree 10 are needed to represent τ and c accurately to machine precision. Also, as seen in Figures 5 and 6 above, other aspects of the solution such as the deviation $\delta_0(t)$ from traveling at a constant speed in conformal space and higher-frequency Fourier modes $\hat{\eta}_{j_1, j_2}$ show greater sensitivity to nonlinear effects than c and τ do.

5. CONCLUSION

In this work, we have formulated the two-dimensional, infinite depth gravity-capillary traveling wave problem in a spatially quasi-periodic, conformal mapping framework. We have numerically demonstrated the existence of traveling solutions, which are a quasi-periodic generalizations of Wilton's ripples. To compute them, we adapted an overdetermined nonlinear least squares technique introduced in [38] for a different problem. For each solution computed, the value of k and the amplitudes of two base Fourier modes $\hat{\eta}_{1,0}$ and $\hat{\eta}_{0,1}$ are fixed while τ , c and the other Fourier modes $\hat{\eta}_{j_1, j_2}$ are varied to search for solutions of (2.34). Before minimizing (3.9), the initial guess for each solution is computed using either the linear approximation (3.11) or numerical continuation. We validate the accuracy of the traveling solutions using the timestepping algorithm of [37]. To evolve at constant speed in physical space, we have shown that the 2d representation of the quasi-periodic waves travel at a nonuniform speed through the torus. We observed resonance effects in the Fourier modes $\hat{\eta}_{j_1, j_2}$ along the line $j_1 + j_2 k = 0$ and computed the nonlinear dependence of phase speed and surface tension for the two-dimensional family with amplitude parameters in the range $\max\{|\hat{\eta}_{1,0}|, |\hat{\eta}_{0,1}|\} \leq 0.01$.

The question of what happens in our framework if k is rational is interesting. We believe the initial value problem (2.25) could still be solved, though in that case solving the torus version of the equations is equivalent to simultaneously computing a family of 1d solutions on a periodic domain. Families of 1d waves corresponding to a single solution of the torus problem are discussed in detail in [37], and take the form (2.28) above. If $k = q/p$ with p

and q relatively prime integers, the waves in this family all have period $2\pi p$. The traveling wave problem becomes degenerate if k is rational — solutions of the torus version of (2.34) may still exist (we do not know), but if so, they are not unique. Indeed, if $k = q/p$ as above and $\tilde{\eta}_1$ solves the torus version of (2.34), then for any 2π -periodic, real analytic function $\alpha_0(r)$,

$$(5.1) \quad \tilde{\eta}_2 \begin{pmatrix} \alpha_1 \\ \alpha_2 \end{pmatrix} = \tilde{\eta}_1 \left(\begin{pmatrix} \alpha_1 \\ \alpha_2 \end{pmatrix} - \begin{pmatrix} p \\ q \end{pmatrix} \alpha_0(-q\alpha_1 + p\alpha_2) \right)$$

will also be a solution of (2.34) since the corresponding 1d functions passing through the torus along characteristic lines are related by a simple reparametrization,

$$(5.2) \quad \eta_2(\alpha; \theta) = \tilde{\eta}_2 \begin{pmatrix} \alpha \\ \theta + k\alpha \end{pmatrix} = \tilde{\eta}_1 \begin{pmatrix} \alpha - p\alpha_0(p\theta) \\ \theta + k\alpha - q\alpha_0(p\theta) \end{pmatrix} = \eta_1(\alpha - p\alpha_0(p\theta); \theta).$$

Another degeneracy is that the modes $\hat{\eta}_{j_1, j_2}$ of a solution of (2.34) with $j_1 + kj_2 = 0$ and $(j_1, j_2) \neq (0, 0)$ can be modified arbitrarily (maintaining $\hat{\eta}_{-j_1, -j_2} = \overline{\hat{\eta}_{j_1, j_2}}$) to obtain additional solutions of (2.34). These modes are plane waves that only affect the 1d functions passing through the torus along characteristic lines by an additive constant. The resonance phenomenon observed in the Fourier modes in Figure 6 is presumably a small-divisor phenomenon [20] in the irrational case related to this degeneracy. If solutions for rational k exist, a natural open question is whether they can be selected to fit together continuously with solutions for nearby irrational wave numbers. In floating point arithmetic, irrational wave numbers are approximated by rational ones. We did not encounter difficulties with this, presumably because the above degeneracies are not visible with the grid resolution used. More work is needed to understand this rigorously.

Our results show that the amplitude ratio $\gamma = \hat{\eta}_{1,0}/\hat{\eta}_{0,1}$ plays an important role in determining the shapes of solutions. As seen in Figures 1 and 3, the quasi-periodic features of the solutions are most evident when $\gamma \approx 1$. In the future, we plan to study the behavior of different perturbation families, e.g. fixing the amplitudes of different base Fourier modes in (2.39) such as $\hat{\eta}_{1,0}$ and $\hat{\eta}_{1,1}$. We also aim to use this methodology to compute spatially quasi-periodic traveling gravity-capillary waves of finite depth, to compute the time evolution of solutions of the finite depth quasi-periodic initial value problem, and to study the stability of spatially quasi-periodic water waves along the lines of what has been done for periodic traveling waves [12, 26] and Wilton ripples [35].

APPENDIX A. DYNAMICS OF TRAVELING WAVES IN CONFORMAL SPACE

In this section we study the dynamics of the traveling waves computed in Section 2.4 under the evolution equations (2.25) for various choices of C_1 . We show that the waves maintain a permanent form but generally travel at a non-uniform speed in conformal space. We start by showing that there is a choice of C_1 for which η and φ remain stationary in time. We then show how C_1 changes when the waves are phase shifted by $\alpha_0(t)$, and how to determine $\alpha_0(t)$ so that C_1 takes the value in (2.26). The evolution of the torus version of (2.34) under (2.25) is also worked out. We will need the following theorem and corollary, proved in [37]:

Theorem A.1. *Suppose $\varepsilon > 0$ and $z(w)$ is analytic on the half-plane $\mathbb{C}_\varepsilon^- = \{w : \text{Im } w < \varepsilon\}$. Suppose there is a constant $M > 0$ such that $|z(w) - w| \leq M$ for $w \in \mathbb{C}_\varepsilon^-$, and that the restriction*

$\zeta = z|_{\mathbb{R}}$ is injective. Then the curve $\zeta(\alpha)$ separates the complex plane into two regions, and $z(w)$ is an analytic isomorphism of the lower half-plane onto the region below the curve $\zeta(\alpha)$.

Corollary A.2. Suppose $k > 0$ is irrational, $\tilde{\eta}(\alpha_1, \alpha_2) = \sum_{(j_1, j_2) \in \mathbb{Z}^2} \hat{\eta}_{j_1, j_2} e^{i(j_1 \alpha_1 + j_2 \alpha_2)}$, and there exist constants C and $\varepsilon > 0$ such that

$$(A.1) \quad \hat{\eta}_{-j_1, -j_2} = \overline{\hat{\eta}_{j_1, j_2}}, \quad |\hat{\eta}_{j_1, j_2}| \leq C e^{-3\varepsilon K \max(|j_1|, |j_2|)}, \quad (j_1, j_2) \in \mathbb{Z}^2,$$

where $K = \max(k, 1)$. Let x_0 be real and define $\tilde{\xi} = x_0 + H[\tilde{\eta}]$, $\tilde{\zeta} = \tilde{\xi} + i\tilde{\eta}$ and

$$(A.2) \quad \tilde{z}(\alpha_1, \alpha_2, \beta) = x_0 + i\hat{\eta}_{0,0} + \sum_{j_1 + j_2 k < 0} 2i\hat{\eta}_{j_1, j_2} e^{-(j_1 + j_2 k)\beta} e^{i(j_1 \alpha_1 + j_2 \alpha_2)}, \quad (\beta < \varepsilon),$$

where the sum is over all integer pairs (j_1, j_2) satisfying the inequality. Suppose also that for each fixed $\theta \in [0, 2\pi)$, the function $\alpha \mapsto \zeta(\alpha; \theta) = \alpha + \tilde{\zeta}(\alpha, \theta + k\alpha)$ is injective from \mathbb{R} to \mathbb{C} and $\zeta_\alpha(\alpha; \theta) \neq 0$ for $\alpha \in \mathbb{R}$. Then for each $\theta \in \mathbb{R}$, the curve $\zeta(\alpha; \theta)$ separates the complex plane into two regions and

$$(A.3) \quad z(\alpha + i\beta; \theta) = (\alpha + i\beta) + \tilde{z}(\alpha, \theta + k\alpha, \beta), \quad (\beta < \varepsilon)$$

is an analytic isomorphism of the lower half-plane onto the region below $\zeta(\alpha; \theta)$. Moreover, there is a constant $\delta > 0$ such that $|z_w(w; \theta)| \geq \delta$ for $\text{Im } w \leq 0$ and $\theta \in \mathbb{R}$.

We now prove a theorem and two corollaries that describe the dynamics of traveling waves in conformal space under the evolution equations (2.25) for various choices of C_1 .

Theorem A.3. Suppose $\tilde{\eta}_0(\alpha_1, \alpha_2)$ satisfies the torus version of (2.34) as well as the assumptions in Corollary A.2. Define $\tilde{\xi}_0 = H[\tilde{\eta}_0]$, $\tilde{\zeta}_0 = \tilde{\xi}_0 + i\tilde{\eta}_0$ and $\tilde{\varphi}_0 = c\tilde{\xi}_0$. Let $\eta_0(\alpha; \theta) = \tilde{\eta}_0(\alpha, \theta + k\alpha)$, $\varphi_0(\alpha; \theta) = \tilde{\varphi}_0(\alpha, \theta + k\alpha)$, $\xi_0(\alpha; \theta) = \alpha + \tilde{\xi}_0(\alpha, \theta + k\alpha)$ and $\zeta_0 = \xi_0 + i\eta_0$. Suppose that for each $\theta \in [0, 2\pi)$, $\alpha \mapsto \zeta_0(\alpha; \theta)$ is injective, i.e. none of the curves in the family (2.37) self-intersect. Then for each $\theta \in \mathbb{R}$,

$$(A.4) \quad \zeta(\alpha, t; \theta) = \zeta_0(\alpha; \theta) + ct, \quad \varphi(\alpha, t; \theta) = \varphi_0(\alpha; \theta)$$

satisfy (2.25) with $C_1 = cP_0[\xi_\alpha/J]$.

Proof. We have assumed the initial reconstruction of ξ from η yields $\xi(\alpha, 0; \theta) = \xi_0(\alpha; \theta)$, so $x_0(0) = 0$ in (2.13). We need to show that $\eta_t = 0$, $\varphi_t = 0$ and $dx_0/dt = c$ in (2.25), from which it follows that $\xi(\alpha, t; \theta) = \xi_0(\alpha; \theta) + ct$. Since $\tilde{\xi}_0 = H[\tilde{\eta}_0]$ and none of the curves in the family (2.37) self-intersect, Theorem A.1 and Corollary A.2 above show that the holomorphic extension from $\zeta_0(\alpha; \theta)$ to $z_0(w; \theta)$ is an analytic isomorphism of the lower half-plane to the fluid region, and $1/|z_{0,w}|$ is uniformly bounded. In (2.25), we define $\xi_\alpha = 1 + H[\eta_\alpha]$, $\psi = -H[\varphi]$, $J = \xi_\alpha^2 + \eta_\alpha^2$ and $\chi = \psi_\alpha/J$. This formula for ξ_α gives the same result as differentiating $\xi(\alpha, t; \theta)$ in (A.4) with respect to α . From $\tilde{\varphi}_0 = c\tilde{\xi}_0$ and $\hat{\eta}_{0,0} = 0$, we have $\chi = c\eta_\alpha/J$. The extension of $\zeta(\alpha, t; \theta)$ to the lower half-plane is $z(w, t; \theta) = [z_0(w; \theta) + ct]$. We have not yet established that $\zeta(\alpha, t; \theta)$ solves (2.25), but we know z_t/z_w is bounded in the lower half-plane, so there is a C_1 such that

$$(A.5) \quad \begin{pmatrix} -H\chi + C_1 \\ -\chi \end{pmatrix} = \frac{1}{J} \begin{pmatrix} \xi_\alpha & \eta_\alpha \\ -\eta_\alpha & \xi_\alpha \end{pmatrix} \begin{pmatrix} c \\ 0 \end{pmatrix},$$

where the right-hand side represents complex division of z_t by z_α . Since $P_0 H\chi = 0$, we learn from (A.5) that $C_1 = cP_0[\xi_\alpha/J]$. But ξ_t and η_t in (2.23) are obtained by multiplying (A.5) by

$[\xi_\alpha, -\eta_\alpha; \eta_\alpha, \xi_\alpha]$, which gives $\xi_t = c$, $\eta_t = 0$. Equation (2.24) is then $dx_0/dt = P_0[\xi_t] = c$. Finally, using $\chi = c\eta_\alpha/J$, $H\chi = C_1 - c\xi_\alpha/J$, $\varphi_\alpha = c(\xi_\alpha - 1)$ and $\psi_\alpha = c\eta_\alpha$ in (2.25) gives

$$\begin{aligned}
 \varphi_t &= P \left[\frac{\psi_\alpha^2 - \varphi_\alpha^2}{2J} - \varphi_\alpha H[\chi] + C_1 \varphi_\alpha - g\eta + \tau\kappa \right] \\
 (A.6) \quad &= P \left[\frac{c^2 \eta_\alpha^2 - c^2 (\xi_\alpha^2 - 2\xi_\alpha + 1)}{2J} + c \frac{c(\xi_\alpha - 1)\xi_\alpha}{J} - g\eta + \tau\kappa \right] \\
 &= P \left[\frac{c^2}{2J} (J - 1) - g\eta + \tau\kappa \right] = P \left[-\frac{c^2}{2J} - g\eta + \tau\kappa \right] = 0,
 \end{aligned}$$

where we used (2.34) in the last step. \square

Corollary A.4. Suppose $\tilde{\zeta}_0(\alpha_1, \alpha_2)$, $\tilde{\varphi}_0(\alpha_1, \alpha_2)$, $\zeta_0(\alpha; \theta)$ and $\varphi_0(\alpha; \theta)$ satisfy the hypotheses of Theorem A.3 and $\alpha_0(t)$ is any continuously differentiable, real-valued function. Then

$$(A.7) \quad \zeta(\alpha, t; \theta) = \zeta_0(\alpha - \alpha_0(t); \theta) + ct, \quad \varphi(\alpha, t; \theta) = \varphi_0(\alpha - \alpha_0(t); \theta)$$

are solutions of (2.25) with $C_1 = cP_0[\xi_\alpha/J] - \alpha'_0(t)$. The corresponding solutions of the torus version of (2.25) for this choice of C_1 are

$$\begin{aligned}
 (A.8) \quad \tilde{\zeta}(\alpha_1, \alpha_2, t) &= \tilde{\zeta}_0(\alpha_1 - \alpha_0(t), \alpha_2 - k\alpha_0(t)) + ct - \alpha_0(t), \\
 \tilde{\varphi}(\alpha_1, \alpha_2, t) &= \tilde{\varphi}_0(\alpha_1 - \alpha_0(t), \alpha_2 - k\alpha_0(t)).
 \end{aligned}$$

Proof. Since ∂_α and H commute with α -translations, substitution of $\eta_0(\alpha - \alpha_0(t); \theta)$ and $\varphi_0(\alpha - \alpha_0(t); \theta)$ in the right-hand sides of (2.25) without changing C_1 would still lead to $\eta_t = 0$, $\varphi_t = 0$ and $dx_0/dt = c$, and (2.23) would still give $\xi_t = c$. Including $-\alpha'_0(t)$ in C_1 leads instead to $\eta_t = -\alpha'_0(t)\eta_\alpha$ and $\varphi_t = -\alpha'_0(t)\varphi_\alpha$ in (2.25) and $\xi_t = c - \alpha'_0(t)\xi_\alpha$ in (2.23), which are satisfied by (A.7). It also leads to $dx_0/dt = [c - \alpha'_0(t)]$ in (2.24), which keeps the reconstruction of ξ from η via (2.13) consistent with the evolution equation for ξ_t .

The functions in (A.7) and (A.8) are related by

$$(A.9) \quad \zeta(\alpha, t; \theta) = \alpha + \tilde{\zeta}(\alpha, \theta + k\alpha, t), \quad \varphi(\alpha, t; \theta) = \tilde{\varphi}(\alpha, \theta + k\alpha, t).$$

Applying the 1d version of (2.25) to (A.9) is equivalent to applying the torus version of (2.25) to (A.8) and evaluating at $(\alpha, \theta + k\alpha, t)$. Since (A.7) satisfies the 1d version of (2.25) and every point $(\alpha_1, \alpha_2) \in \mathbb{T}^2$ can be written as $(\alpha, \theta + k\alpha)$ for some α and θ , (A.8) satisfies the torus version of (2.25). \square

Corollary A.5. Suppose $\tilde{\zeta}_0(\alpha_1, \alpha_2)$, $\tilde{\varphi}_0(\alpha_1, \alpha_2)$, $\zeta_0(\alpha; \theta)$ and $\varphi_0(\alpha; \theta)$ satisfy the hypotheses of Theorem A.3 and $\xi_{0,\alpha}(\alpha; \theta) > 0$ for $\alpha \in [0, 2\pi)$ and $\theta \in [0, 2\pi)$. Then if C_1 is chosen as in (2.26) to maintain $\tilde{\xi}(0, 0, t) = 0$, the solution of the torus version of (2.25) with initial conditions

$$(A.10) \quad \tilde{\zeta}(\alpha_1, \alpha_2, 0) = \tilde{\zeta}_0(\alpha_1, \alpha_2), \quad \tilde{\varphi}(\alpha_1, \alpha_2, 0) = \tilde{\varphi}_0(\alpha_1, \alpha_2)$$

has the form (A.8) with

$$(A.11) \quad \alpha_0(t) = ct - \mathcal{A}(-ct, -kct),$$

where $\mathcal{A}(x_1, x_2)$ is defined implicitly by

$$(A.12) \quad \mathcal{A}(x_1, x_2) + \tilde{\xi}_0(x_1 + \mathcal{A}(x_1, x_2), x_2 + k\mathcal{A}(x_1, x_2)) = 0, \quad (x_1, x_2) \in \mathbb{T}^2.$$

Proof. The assumption that $\xi_{0,\alpha}(\alpha; \theta) > 0$ ensures that all the waves in the family $\zeta_0(\alpha; \theta)$ are single-valued and have no vertical tangent lines. Under these hypotheses, it is proved in [37] that there is a unique function $\mathcal{A}(x_1, x_2)$ satisfying (A.12) and that it is real analytic and periodic. We seek a solution of the form (A.8) satisfying $\tilde{\xi}(0, 0, t) = 0$,

$$(A.13) \quad \begin{aligned} \tilde{\xi}(0, 0, t) &= \tilde{\xi}_0(-\alpha_0(t), -k\alpha_0(t)) + ct - \alpha_0(t) \\ &= [ct - \alpha_0(t)] + \tilde{\xi}_0(-ct + [ct - \alpha_0(t)], -kct + k[ct - \alpha_0(t)]) = 0. \end{aligned}$$

Comparing with (A.12), we find that $[ct - \alpha_0(t)] = \mathcal{A}(-ct, -kct)$, which is (A.11). Since $\tilde{\eta}_0(\alpha_1, \alpha_2)$ is even, $\tilde{\xi}_0 = H[\tilde{\eta}_0]$ is odd and $\mathcal{A}(0, 0) = 0$. Thus, $\alpha_0(0) = 0$ and the initial conditions (A.10) are satisfied. Since $\xi(0, 0, t) = 0$, C_1 satisfies (2.26). \square

REFERENCES

- [1] Benjamin F Akers and Wenxuan Gao. Wilton ripples in weakly nonlinear model equations. *Communications in Mathematical Sciences*, 10(3):1015–1024, 2012.
- [2] David M Ambrose and Jon Wilkening. Computation of symmetric, time-periodic solutions of the vortex sheet with surface tension. *Proceedings of the National Academy of Sciences*, 107(8):3361–3366, 2010.
- [3] David M Ambrose and Jon Wilkening. Dependence of time-periodic vortex sheets with surface tension on mean vortex sheet strength. *Procedia IUTAM*, 11:15–22, 2014.
- [4] Sheldon Axler, Paul Bourdon, and Wade Ramey. *Harmonic Function Theory*. Springer-Verlag, New York, 1992.
- [5] Pietro Baldi, Massimiliano Berti, Emanuele Haus, and Riccardo Montalto. Time quasi-periodic gravity water waves in finite depth. *Inventiones mathematicae*, 214(2):739–911, 2018.
- [6] J Thomas Beale. The existence of cnoidal water waves with surface tension. *Journal of Differential Equations*, 31(2):230–263, 1979.
- [7] Massimiliano Berti and Riccardo Montalto. Quasi-periodic standing wave solutions of gravity-capillary water waves. *arXiv preprint arXiv:1602.02411*, 2016.
- [8] TJ Bridges and F Dias. Spatially quasi-periodic capillary-gravity waves. *Contemporary Mathematics*, 200:31–46, 1996.
- [9] Wooyoung Choi and Roberto Camassa. Exact evolution equations for surface waves. *Journal of engineering mechanics*, 125(7):756–760, 1999.
- [10] W. Craig and C. Sulem. Numerical simulation of gravity waves. *J. Comp. Phys.*, 108:73–83, 1993.
- [11] A. D. D. Craik. George Gabriel Stokes on water wave theory. *Annual Rev. Fluid Mech.*, 37:23–42, 2005.
- [12] B. Deconinck and K. Oliveras. The instability of periodic surface gravity waves. *J. Fluid Mech.*, 675:141–167, 2011.
- [13] Alexander I Dyachenko, Evgenii A Kuznetsov, MD Spector, and Vladimir E Zakharov. Analytical description of the free surface dynamics of an ideal fluid (canonical formalism and conformal mapping). *Physics Letters A*, 221(1-2):73–79, 1996.
- [14] Alexander I Dyachenko, Vladimir E Zakharov, and Evgenii A Kuznetsov. Nonlinear dynamics of the free surface of an ideal fluid. *Plasma Physics Reports*, 22(10):829–840, 1996.
- [15] S.A. Dyachenko, P.M. Lushnikov, and A.O. Korotkevich. Branch cuts of stokes wave on deep water. part I: Numerical solution and Padé approximation. *Stud. in Appl. Math*, 2016.
- [16] Sergey A Dyachenko, Pavel M Lushnikov, and Alexander O Korotkevich. Branch cuts of stokes wave on deep water. part i: numerical solution and padé approximation. *Studies in Applied Mathematics*, 137(4):419–472, 2016.
- [17] Sanjay Govindjee, Trevor Potter, and Jon Wilkening. Cyclic steady states of treaded rolling bodies. *International Journal for Numerical Methods in Engineering*, 99(3):203–220, 2014.
- [18] T. Y. Hou, J. S. Lowengrub, and M. J. Shelley. Removing the stiffness from interfacial flows with surface tension. *J. Comput. Phys.*, 114:312–338, 1994.
- [19] T. Y. Hou, J. S. Lowengrub, and M. J. Shelley. The long-time motion of vortex sheets with surface tension. *Phys. Fluids*, 9:1933–1954, 1997.

- [20] Gérard Iooss and Pavil I Plotnikov. *Small divisor problem in the theory of three-dimensional water gravity waves*. American Mathematical Soc., 2009.
- [21] R. S. Johnson. *A modern introduction to the mathematical theory of water waves*. Cambridge University Press, Cambridge, UK, 1997.
- [22] Mark Jones and John Toland. Symmetry and the bifurcation of capillary-gravity waves. In *Analysis and Continuum Mechanics*, pages 357–381. Springer, 1989.
- [23] Horace Lamb. *Hydrodynamics*. Dover, 6th edition, 1932. *A treatise on the Mathematical Theory of the Motion of Fluids*, 1879.
- [24] Tullio Levi-Civita. Determination rigoureuse des ondes permanentes d’amplitude finie. *Mathematische Annalen*, 93(1):264–314, 1925.
- [25] Yi A Li, James M Hyman, and Wooyoung Choi. A numerical study of the exact evolution equations for surface waves in water of finite depth. *Studies in applied mathematics*, 113(3):303–324, 2004.
- [26] R. S. MacKay and P. G. Saffman. Stability of water waves. *Proc. R. Soc. Lond. A*, 406:115–125, 1986.
- [27] Daniel I Meiron, Steven A Orszag, and Moshe Israeli. Applications of numerical conformal mapping. *Journal of Computational Physics*, 40(2):345–360, 1981.
- [28] P. A. Milewski, J.-M. Vanden-Broeck, and Z. Wang. Dynamics of steep two-dimensional gravity–capillary solitary waves. *J. Fluid Mech.*, 664:466–477, 2010.
- [29] L. M. Milne-Thomson. *Theoretical Hydrodynamics*. MacMillan, London, 5th edition, 1968.
- [30] Aleksandr I Nekrasov. On steady waves. *Izv. Ivanovo-Voznesensk. Politekh. In-ta*, 3:52–65, 1921.
- [31] Jorge Nocedal and Stephen J. Wright. *Numerical Optimization*. Springer, New York, 1999.
- [32] Chris H Rycroft and Jon Wilkening. Computation of three-dimensional standing water waves. *Journal of Computational Physics*, 255:612–638, 2013.
- [33] G. G. Stokes. On the theory of oscillatory waves. *Trans. Camb. Philos. Soc.*, 8:441–455, 1847.
- [34] John Francis Toland and MCW Jones. The bifurcation and secondary bifurcation of capillary-gravity waves. *Proceedings of the Royal Society of London. A. Mathematical and Physical Sciences*, 399(1817):391–417, 1985.
- [35] O. Trichtchenko, B. Deconinck, and J. Wilkening. The instability of Wilton’s ripples. *Wave Motion*, 66:147–155, 2016.
- [36] Jean-Marc Vanden-Broeck. *Gravity–Capillary Free–Surface Flows*. Cambridge University Press, Cambridge, 2010.
- [37] J. Wilkening and X. Zhao. Spatially quasi-periodic water waves of infinite depth. 2020. (submitted).
- [38] Jon Wilkening and Jia Yu. Overdetermined shooting methods for computing standing water waves with spectral accuracy. *Computational Science & Discovery*, 5(1):014017, 2012.
- [39] JR Wilton. On ripples. *The London, Edinburgh, and Dublin Philosophical Magazine and Journal of Science*, 29(173):688–700, 1915.
- [40] V. E. Zakharov. Stability of periodic waves of finite amplitude on the surface of a deep fluid. *Zhurnal Prikladnoi Mekhaniki i Tekhnicheskoi Fiziki*, 8:86–94, 1968.
- [41] Vladimir E Zakharov, Alexander I Dyachenko, and Oleg A Vasilyev. New method for numerical simulation of a nonstationary potential flow of incompressible fluid with a free surface. *European Journal of Mechanics-B/Fluids*, 21(3):283–291, 2002.
- [42] Juan Antonio Zufiria. *Part I: Symmetry Breaking of Water Waves. Part II: On the superharmonic instabilities of surface water waves*. PhD thesis, California Institute of Technology, April 1987.

DEPARTMENT OF MATHEMATICS, UNIVERSITY OF CALIFORNIA AT BERKELEY, BERKELEY, CA, 94720, USA

E-mail address: wilkening@berkeley.edu

E-mail address: zhaoxinyu@berkeley.edu